

APPENDIX E

The Regional Meteorological Model Status Report

by

James E. Overland

September 1978

A major limitation of pollutant trajectory modeling is the inadequate specification of the local "wind field at the spatial resolution necessary to resolve wind drift. Typically, this is due to difficulty of estimating nearshore wind fields directly from large scale synoptic patterns or widely scattered and often unrepresentative wind measurements. Near the coastline of Alaska topography and discontinuities in surface roughness and heating give rise to significant mesoscale variations.

A numerical meteorological model has been developed for use in conjunction with a field measurement program to ascertain the magnitude of mesoscale modification and aid in determining regional wind patterns. A full description of the model is given in the attached PMEL Technical Report (in press). Within the context of its formulation, the model can be used to assess the implications of changes in large scale flow, surface parameters, and assumed dynamics on the wind pattern in a limited region. A major goal is the ability to infer local winds and small scale spatial variations in wind fields from the large scale flow pattern for locations where long term direct observations are not practical.

The model chosen is an adaptation of one proposed by Lavoie which consists of fairly general conservation statements for mass, momentum, and heat. Lavoie treats the planetary boundary layer (PBL), typically 0.5 to 2 km deep, as a one layer, vertically integrated primitive equation model. The model solves for the two components of horizontal velocity, boundary layer height, and potential temperature throughout a limited region. Large scale geostrophic wind, surface elevation, temperature, and the stability of the air in the layer above the PBL are specified as boundary conditions. Air temperature and PBL height are specified along the inflow boundaries. The local response is calculated by specifying smooth initial values of wind,

temperature and PBL height and then time stepping the equations of continuity, momentum, and heat conservation until an equilibrium state is obtained. The system is free to estimate mesoscale wind variations caused by contrasts in heating and roughness of land and water, modification of the down wind environment by advection and channeling by topography. The equilibrium state is considered to give the local winds which occur in conjunction with the given large scale pressure pattern.

The model consists of only one layer processes which depend upon vertical structure that cannot be directly resolved; however, the model is well suited to estimating wind patterns in mountainous regions with strong orographic control. For example, questions remain on the adequacy of the model to represent sea breeze circulation without explicitly resolving return flow aloft or katabatic flows that occur within a planetary boundary layer.

The Puget Sound - Strait of Juan de Fuca region in northwest Washington State was used as a test basin as a fairly comprehensive data set was obtained for initial comparison. Complete description of three case studies is also included in the Technical Report. In applying the model to Puget Sound it was determined that the model was very well suited for studying the interaction of inertia and orographic channeling; specifically the continuity balance resulting from air coming into the basin from two directions and ability to resolve mesoscale eddies shed by headlands. There were two shortcomings of the model. The first is that air stability (the restoring force in the model) is applied only at the top of the boundary layer. Several synoptic situations consisted of continuously stratified conditions. These can be simulated (as opposed to modeled) by a very shallow PBL with a strong jump at the top. The other problem is treating open boundary conditions along and edge that contains a land-water transition. The PBL height must be

a priori along an open boundary and it is not known ahead of time what the PBL modification is for onshore flow. This problem **was solved** in part by iteration. To resolve stable atmospheric cases, making the model more complicated in terms of number of layers, adding mass entrainment across the top of the PBL, etc., would have an adverse impact upon resolving the dominant physics of channeling and treatment **and** initialization of open boundaries. In **summary**, the model is very good at looking at certain dominant meteorological features (which we think are important) but not **all** features. However, more complicated models are not the answer to providing better winds as certain meteorological processes cannot be effectively modeled simultaneously.

The first application of the regional meteorological model (RMM) to Alaska was for the Icy Bay - Yakutat vicinity (Figure 1). It showed extensive channeling over the mountains and a transition of the coastal flow to the offshore **geostrophically** balanced winds. It was less successful in explaining thermodynamically driven features and suffered **from** questions of what were the appropriate boundary conditions along the eastern edge of the model. About this time the format for the winds input to the trajectory calculations were finalized. The region was all of **NEGOA** at a scale coarser than the RMM. As the preliminary runs of the RMM were **supportive of the general conclusions of Reynolds (RU #367) on the offshore extent of the coastal zone and the katabatic zone, further runs of the RMM were not necessary. Establishing these length scales was adequate spatial information on coastal wind modification** for the trajectory model.

Attention was then turned to applying the RMM to Kodiak Island and Lower Cook Inlet (LCI). This has **been accomplished**. Figures 2 and 3 show two arrow plots for two **geostrophic** offshore wind directions of 155° and 180°. Kodiak Island is in the lower part of the figure. Points denoted by

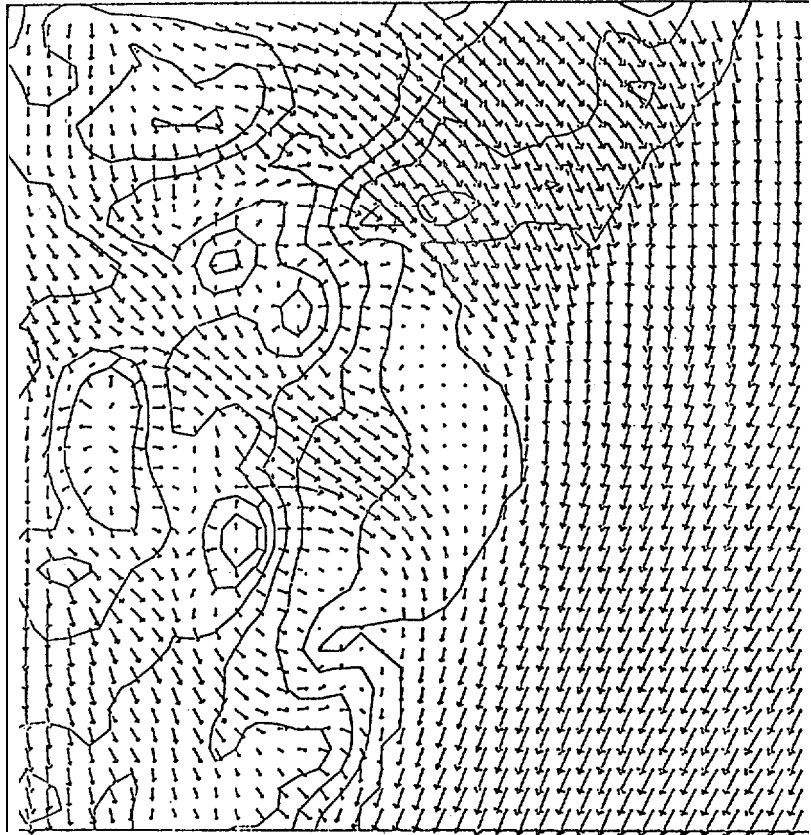


Figure 1

an "x" imply that the ground elevation is higher than the marine planetary boundary layer. The high steep mountains make an ideal location for the RMM. Figure 2 has a piling up of air along the **open coast** and at the entrance **to Shelikof Strait** (lower left). This causes channeling **into the Strait** at a large angle to the incident wind from the southeast. The jet formed at the eastern coast continues halfway into LCI under the influence of inertia. Figure 3 has the incident wind rotated 25° to the south **relative to Figure 2**. Flow in upper Cook Inlet. Figure 4 shows a sample arrow **plot** for the Kodiak grid. It has many of the same advantages for the RMM as LCI.

The RMM is at the stage for both **LCI** and Kodiak to be an aid in **interpreting the field measurements with RU #367** in a comprehensive review of **LCI**.

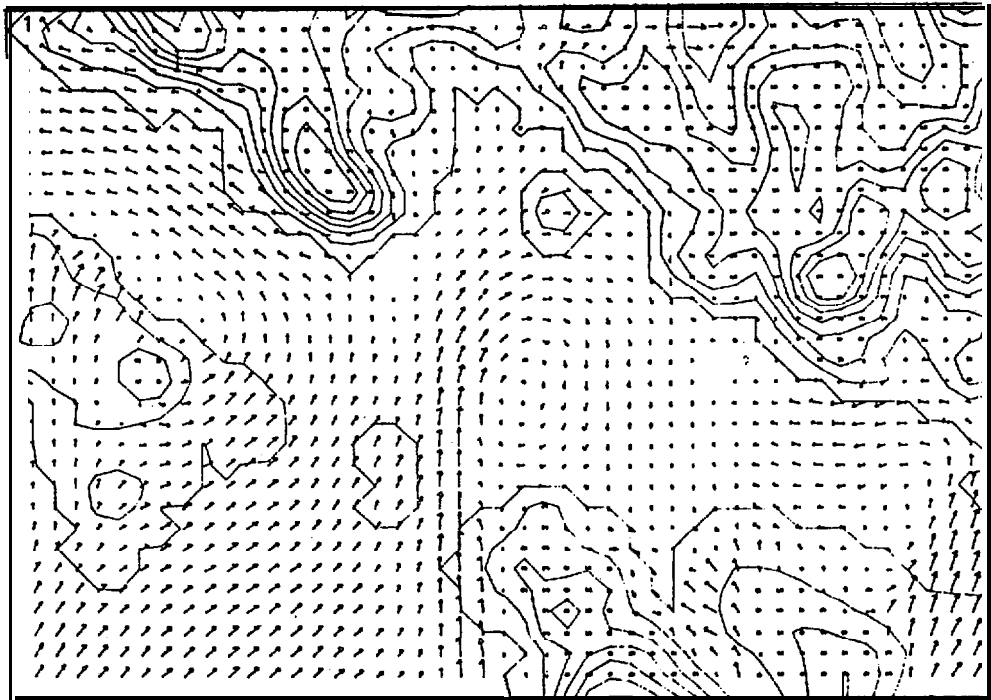


Figure 2

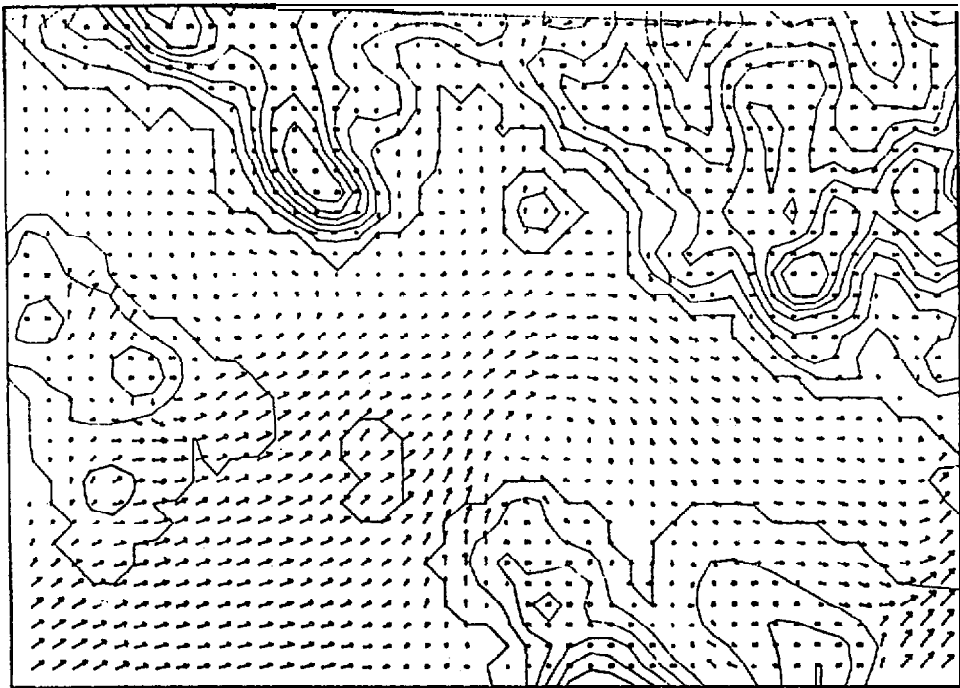


Figure 3

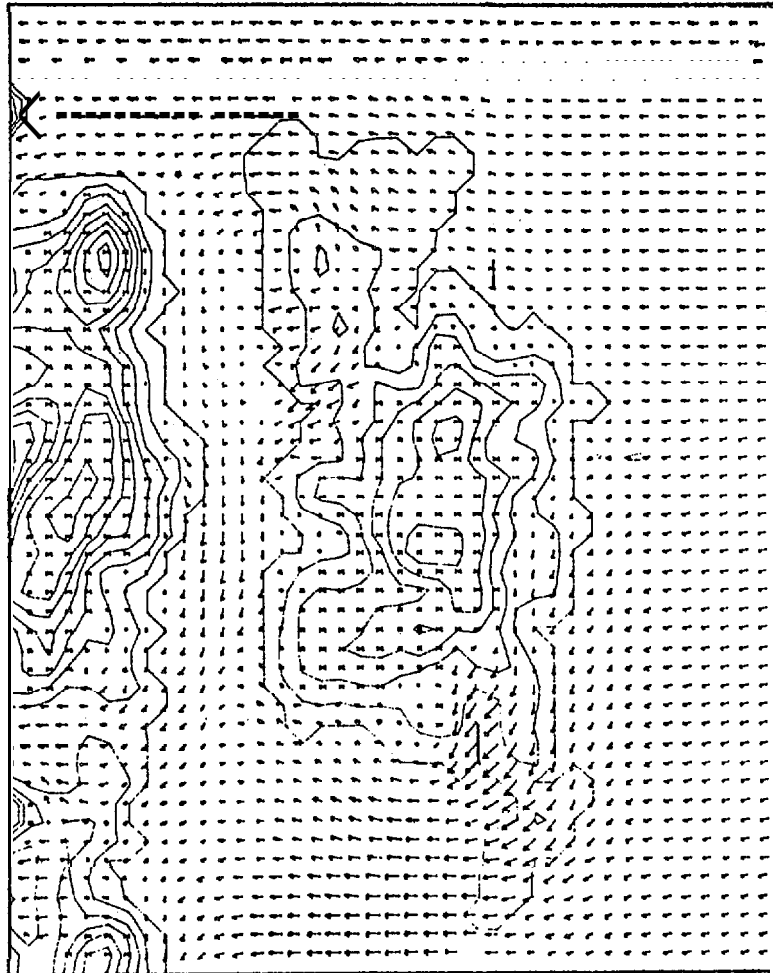


Figure 4

A Regional Surface Wind Model
for Mountainous Coastal Areas

by

James E. Overland, Matthew H. Hitchman,
and Young June Han

(Contribution No. 366 from the NOAA/ERL
Pacific Marine Environmental Laboratory.)

1978

TABLE OF CONTENTS

	Page
ABSTRACT.	621
1. INTRODUCTION.	622
2. THE MODEL	625
3. DETAILS	628
3.1 Finite Difference Form	628
3.2 Boundary Conditions.	628
3.3 Flooding	629
3.4 Entrainment.	630
3.5 Initialization	630
4. SIMPLE EXPERIMENTS.	631
5. SIMULATION FOR PUGET SOUND-STRAIT OF JUAN DE FUCA	637
5.1 Regional Description	638
5.2 Data Sources	640
5.3 Meteorological Case Discussion	642
6. ACKNOWLEDGEMENTS.	649
7. REFERENCES.	650
APPENDIX A: Derivation of Boundary Layer Equations	651
FIGURES.	654

ABSTRACT. The **Mesoscale** Numerical Model of the Planetary Boundary Layer (PBL) which Lavoie applied to lake-effect snowstorms is modified for maritime application **in orographically** dominated regions along the west coast of the United States and along the coast of southern Alaska. The model treats the PBL as a **one-**layer primitive equation system solving for the two components of horizontal velocity, boundary layer height, and potential temperature throughout a limited region, subject to specification **of the** large-scale geostrophic wind pattern and the stability of the air above the PBL.

Experiments with a cross-section version of the model are performed to assess the model's response to variable terrain, differential heating, and differential roughness at the coast for a domain containing both a flat coastal plain and **low** coastal mountains such as the shore along Oregon.

The complete model is applied to three quite dissimilar synoptic situations for the **Puget** Sound-Strait of Juan de Fuca system **in** northwest Washington State. The model is specifically useful **in** suggesting the dynamic and kinematic causes of the complex flow **patterns observed in** each regime, particularly the relative role of inertia and topography.

1. INTRODUCTION

A major limitation of coastal marine meteorology is the inadequate specification of the **local** wind field at the spatial resolution necessary to resolve wind drift, local waves, and **vessel** or oil spill leeway. Typically, this is due to the difficulty of estimating nearshore **wind fields** directly from large-scale synoptic patterns or from widely scattered and often unrepresentative wind measurements. Near the coastline, topography and **discontinuities** in surface roughness and heating give rise to significant **mesoscale** variations. For example, Figure 1 shows reported regions of anomalous wind speed and direction **along** the Alaskan coast. The Alaska region of the National Weather Service compiled Figure 1 from a survey of the Coast Guard and other groups operating vessels in Alaskan waters. **Strong ageostrophic** winds exist in the passes of the southeast Alaskan coast and are attributed to channeling around islands. The open coast is **also** subject to anomalous winds caused **by high** coastal mountains. Of particular importance are winds **blowing** off the land, called **katabatic** winds, forced **by** the contrast of warm ocean temperatures and cold temperatures 50-100 km inland. Further south, in the **Puget** Sound Basin of the State of Washington, forecasters are aware of a quiet zone of reduced winds in the lee of the Olympic Mountains. This zone changes location as a function of the offshore wind direction. Sea breeze circulation is an additional example of coastal modification.

This report documents a numerical meteorological **model** for use in conjunction with a field measurement program to determine regional wind patterns. Within the context of its formulation, the model can **be** used to assess the implications of changes in large-scale flow, surface parameters,

and assumed dynamics on the wind pattern **in** a **limited** region. A major **goal** is the ability to infer local winds and small-scale spatial variations **in** wind fields from the large-scale flow pattern for locations where **long-term** observations are not practical.

We have chosen to adapt a model proposed by Lavoie (1972, 1974; see also Keyser and Anthes, 1977) which consists of fairly general conservation statements for mass, momentum, and heat. Lavoie treats the planetary boundary layer (**PBL**), typically 0.5-2 km deep, as a one-layer, vertically integrated primitive equation model. The model solves for the two components of horizontal velocity, boundary layer height, and potential temperature throughout a limited region. Large-scale **geostrophic** wind, surface elevation, temperature, and the stability of the air in the **layer** above the **PBL** are specified as boundary conditions. Air temperature and PBL height are specified along the inflow boundaries. The local response is calculated by specifying smooth initial values of wind, temperature, and PBL height and then time-stepping the equations of continuity, momentum, and heat conservation until an equilibrium state is obtained. The system allows estimation of **mesoscale** wind variations caused by contrasts in heating and roughness of land and water, modification of the down-wind environment by advection and channeling by topography. The equilibrium state is considered to provide the **local** winds which occur in conjunction with the given large-scale pressure patterns. Since the model consists of only one layer, processes which depend upon vertical structure cannot be directly resolved. For example, questions remain on the adequacy of the model to represent sea breeze circulation without explicitly resolving return flow aloft. However, the model is **well** suited

to **estimating** wind patterns in mountainous regions with strong orographic control.

We proceed with the formulation and initial testing of the model. The Puget Sound-Strait of Juan de Fuca region in northwest Washington is used as a test basin because there was a fairly comprehensive data set available for comparison. Since the model is quickly dominated by complex topography, several cases with simple geometry are included in Section 4 to build confidence in interpreting more complicated results. The question of the type and quality of large-scale pressure field input is also addressed by comparison of hand-drawn analyses with machine-prepared analyses from the National Meteorological Center.

2, THE MODEL

The atmosphere is represented by three layers defined by changes in the lapse rate of potential temperature, as shown in Figure 2. The layer in contact with the surface is a constant stress or surface layer assumed to be represented by a logarithmic velocity profile. The upper limit of this layer is taken to be 50 m. Above the surface layer is the planetary boundary layer (PBL), represented by vertically integrated values of velocity and potential temperature, capped by a density discontinuity, which parameterizes the restoring force of an inversion layer of stable air above the PBL. The PBL layer, then, is the only layer which is explicitly modeled. The model specifies four dependent variables: the PBL height, h , identified with the inversion base in unstable or neutral stratification; the PBL potential temperature, θ ; and the two components of the vertically integrated wind velocity within the PBL, \vec{v} . The governing equations for conservation of mass, momentum and heat result from vertically integrating the primitive equations for the PBL, treating the lower atmosphere as a Boussinesq system. Interactions with the surface layer and upper atmosphere are parameterized. The resulting equations (see Appendix A) reduce to:

$$\frac{\partial h}{\partial t} + \nabla \cdot (h-D) \vec{v} = E, \quad (1)$$

$$\begin{aligned} \frac{\partial (h-D) \vec{v}}{\partial t} + \nabla \cdot (h-D) \vec{v} \vec{v} + (h-D) f \vec{k} \times \vec{v} = \\ -(h-D) F_i + \frac{g(h-D) \Delta \theta}{\theta_o} \nabla h + \frac{g(h-D)^2}{2\theta_o} \nabla \theta + E \vec{v}_+ - C_D |\vec{v}| \vec{v}, \end{aligned} \quad (2)$$

$$\frac{\partial (h-D) \theta}{\partial t} + \nabla \cdot (h-D) \vec{v} \theta = E \theta_+ - C_H |\vec{v}| (e - \theta_s). \quad (3)$$

The right side of the mass conservation equation (1) represents the recruitment of mass into the PBL through entrainment of the overlying fluid at rate E . The height of the top of the surface layer above sea level is indicated by D , so that $h-D$ is the local PBL thickness. In the momentum equation (2), the second term is inertia; f is the Coriolis parameter; g is gravity; θ_0 is a reference temperature; \vec{v}_+ is the velocity at the base of the inversion layer (entrained into the PBL at rate E), and CD is the surface drag parameter. The temperature increase between the PBL and the inversion layer is $\Delta\theta$. The air stability associated with the inversion is thus modeled as a jump condition in density. F_1 represents the uniform pressure gradient associated with the background large-scale flow (the major meteorological input to the model), while the next two terms consider pressure gradients developed by the model induced by the local variations in PBL height and temperature. In the absence of mesoscale variation, (2) reduces to a geostrophic balance modified by surface drag. The right-hand side of the heat equation (3) indicates that the PBL can be warmed by entrainment at the top of the PBL (θ_+ being the temperature at the base of the inversion) or by surface heating proportional to the difference between the PBL air temperature and surface temperature, θ_s .

The wind velocity \vec{v} is an average for the entire PBL. Since almost all wind shear is confined to the surface layer, the model wind can be taken as nearly equal to the wind at 50 m elevation. At this level the wind speed is approximately 20% greater than the wind measured at the normal anemometer height of 10 m. Corrected for height in this manner, the model winds should correspond to 10-min averaged anemometer winds which are not unduly influenced by surface features smaller than the mesh length of the model for a well-mixed PBL.

For domain sizes on the order of several hundred kilometers it is important to emphasize the gravitationally controlled circulation, which requires specification of either boundary layer height or inflow velocity. Along inflow boundaries over the ocean, we have chose to specify constant PBL height, h_i , and air temperature θ_i . These values are held fixed for all time. Inflow boundaries over land specify the PBL height and temperature as

$$h = h_i + aD, \quad a = 0.5$$

$$\theta = \theta_i \tag{4}$$

subject to a minimum PBL height. This minimum is now 300 m. After the h values are set by (4), they are smoothed twice by a 1-2-1 smoother to remove the influence of rapid variations in the ground elevation D . Presently, the model needs to be rerun on a case-by-case basis adjusting the constant "a" to minimize the influence of the open boundary on the height field at interior points. The authors are currently experimenting with setting the PBL height along inflow boundaries from the results of a 1-D model, At outflow boundaries we follow Lavoie by setting the PBL height and potential temperature at their upstream values.

3. DETAILS

3.1 Finite Difference Form

The chosen grid is a single Richardson lattice (Figure 3) in which the two velocity components are staggered relative to the height field and each other, with u and v components midway between height points along the x and y axes respectively. This approach is optimal for gravity waves. **This lattice also eliminates overspecification of boundary conditions, a difficulty with Lavoie's original formulation.** The flux form of the advective terms maintains conservation of scalar quantities. Upstream values instead of centrally averaged values for advected quantities are chosen to maintain the transportive property, which guarantees one-way flow of information.

3.2 Boundary Conditions

Specification of boundary conditions for limited area integrations of the **primitive equations** is a formidable task. *one* advantage of the present approach is that constant values on the boundaries can be specified, with the integration run until **all** the ringing of the time-dependent modes is frictionally damped.

Specifying the momentum flux through the open boundaries for the non-linear advection terms in the momentum equations must be done with care, since advection in a limited domain scale is significant. Several options for inflow velocities were investigated, including specifying the laterally homogeneous solution for the given **geostrophic** wind and drag coefficient. This proved unsatisfactory because the imbalance between the boundary values and the internal values influenced by orography caused severe **geostrophic** adjustment problems throughout the model domain and resulted in large deviations in the height field. Our final choice is to assume zero gradient conditions on the velocity components at the inflow boundary. This assumption results in determination of the values at the first interior point by the local dynamic balance. This decision **is** consistent with the limited data input available and the desire to resolve orographic control interior to the model. Since upstream differencing is used for momentum advection, only minor difficulties are encountered at outflow boundaries.

3.3 Flooding

In the presence of high mountains or low mean velocities, the top of the marine inversion layer may actually intersect the topography. **In terms** of the vertically integrated model, this is equivalent to forming an island.

In the cases studied by **Lavoie** it was not necessary to resolve this feature, but it becomes important to resolve for **Puget** Sound and especially for the high Alaskan coastal mountains. In the present model flooding is accomplished by selectively removing a grid point if the **PBL** depth **falls below** a preset value, and adding points if the surrounding PBL heights are great enough to increase the PBL depth above a minimum. Since adding or dropping points creates new internal boundary conditions, flooding increases the relaxation time to steady state by a factor of three.

3.4 Entrainment

Even in the absence of topography, determination of the PBL height is a complex problem. For unstable boundary layers the height cannot be explicitly determined, but is governed by a rate equation which considers free and forced convection, large-scale subsidence, shear instabilities, and solar radiation. The importance of entrainment is problem-dependent and we can suppose that it is more significant in the winter Gulf of Alaska case with cold air outbreaks over warm water than for the Puget Sound case.

In our initial application to mountainous regions we will assume that an oceanic PBL height can be specified *a priori* and, for the time interval necessary for a parcel to flow through the domain of the model, that no significant modification is contributed directly through entrainment, i.e., E is set to zero. Entrainment can be added to this type of model (Stun, 1976, for example), but represents a major complication and is of secondary importance relative to the influence of large topographic features.

3.5 Initialization

The values of parameters and input conditions in Table 1 are used in subsequent model runs.

The background large-scale pressure gradient, \vec{F}_i , is calculated to balance the specified geostrophic wind, V_g . The PBL height is initialized by h_i and velocities are initialized by 70% of the geostrophic wind.

4. SIMPLE EXPERIMENTS

In the sections to follow, complex topography dominates the flow field through the overlapping influence of several mountains and **land/water** contrasts. These **all** contribute to local modification of the wind field. To aid in interpretation of more complex results, this section describes several experiments with simple topography, isolating particular physical processes. The examples use a one-dimensional version of the model (i.e., **north-south derivatives are set to zero**) with the parameters given in **Table 1**. **Topography consists of either a flat coastal plain or coastal mountain 700 m** in elevation. The **latter topography runs west-east and is roughly comparable** to a slice through the Coast Range and **Willamette Valley** in Oregon. The total domain is **large** (300 km) to reduce the influence of the inflow or outflow boundaries. The grid mesh is 3 km. While most of the conclusions in this section can be derived from analytic solutions or scale **analysis**, we take the numerical approach consistent with development of the 2-0 model .

Figure 4a shows the simplest case of onshore flow for a flat coastline. Geostrophic wind approaches from 270° at 13.0 m/s with a boundary layer height of 600 m and no land/water temperature contrast. Seaward, the horizontally homogeneous solution matches the analytical solution for a momentum integral (Brown, 1974) with the boundary layer wind 0.96 of geostrophic and an inflow angle of 17°. Coastal influence begins near the shoreline and, inland, results in a PBL height increase of 260 m and a reduction in wind speed to 9.0 m/s. One measure of the relaxation distance for the flow to return to a near geostrophic-frictional balance is given by the ratio of the magnitude of the inertia terms ($u\partial u/\partial x$, etc.) to the large-scale pressure gradient force ($f\vec{V}_g$). This ratio is given as the top curve in Figure 4a; it is largest just landward of the coast and is 0.1 inland a distance of 100 km. Near the outflow boundary the solution again fits Brown's solution with the increased drag coefficient over land. For mass continuity in a 1-D model with no entrainment, the product of the u-velocity component and the PBL depth must be constant throughout the model domain. In the example of Figure 4a, conservation is satisfied to better than 0.2%.

The importance of momentum advection is further illustrated by contrasting 4a with 4b. In Figure 4b, the same conditions are specified as in 4a, except that the momentum advection terms are set to zero, leaving large-scale and locally induced pressure gradients and friction as the only forces. The seaward extent of coastal influence is much greater. The **main feature is a coastal jet induced** by the rise in the PBL height of 14.5 m/s from 226°, nearly a 65° change from the offshore direction. The second **main feature is a nearly complete frictional equilibrium landward of the coastline. Clearly, in the absence of heating and mountains, inertia dominates onshore** flow resulting in **almost** no modification of the marine wind until right at the coastline. The third example (Figure 4c) is a "sea breeze" with a background **geostrophic** wind of 3.0 m/s from 290°. The land temperature is 291° K, 10° warmer than the ocean. The temperature equilibrates **to** 90% of the temperature contrast 100 km inland from the coast. There is **little** variation in direction except for a delayed frictional turning inland. The wind speed is maximum at the coastline in response to pressure gradient induced by the land-water temperature difference. Continuity in this model requires a lowering of the PBL height in the vicinity of the coast as a result of the increased **velocity**; the resulting slope of the PBL height influences the winds 40 km seaward of the coast. An interesting feature is the double peak in the magnitude of the inertia terms,

Figure 5a shows an offshore wind for the same parameters as in 4a. There is acceleration across the coastline with a maximum 6 km offshore. Acceleration terms still account for 20% of the magnitude of the geostrophic term at the limit of the model, 180 km seaward of the coast. Velocities over land are in frictional equilibrium but they gradually increase offshore to a super-geostrophic magnitude of 14.6 m/s at a distance of 110 km from the coast. A gradual decline is indicated near the limit of the model domain. For an overwater drag coefficient of 1.5×10^{-3} , the boundary layer has only begun to equilibrate with surface friction within the model domain. One can project that coastal influences of offshore flow extend seaward at least 300-500 km. This length scale is further substantiated by the "land breeze" case shown in 5b, in which the ocean is 10°K warmer than the land. The air temperature increases only 3°K over a distance of 180 km. The contribution of the land breeze increase over the background flow is of order 1 m/s, compared to the sea breeze-induced increase of 3 m/s. The length scale for thermal equilibrium of a coastal temperature discontinuity is well beyond the domain of the model even for modest advective velocities on the order of 4 m/s.

The case of a coastal mountain, Figure 6, shows onshore flow for three options of offshore PBL height and no temperature contrast. Even for moderate terrain the results are qualitatively very dissimilar to the flat coastal plain. All three cases show similar patterns of a coastal influence zone that extends from 50 km to 100 km offshore. The offshore transition is not gradual, but is marked by a sharp front at the seaward limit as seen in the PBL height and magnitude of the advective terms. Within this "offshore coastal zone" the winds are reduced by as much as 40% with a minimum approximately 20-40 km offshore. The winds veer to the southwest as they approach the coastline and accelerate toward a minimum in the PBL height on the lee side of the mountain. They then recover to a near-frictional balance within 50 km of the PBL minimum. Figure 7 shows the influence of the presence of the mountain on sea breeze circulation (10°K land/sea temperature contrast). In this formulation the mountain acts as an effective barrier to development and emphasizes the importance of low-level valleys in the mountain range for the development of sea breeze circulation. In addition to temperature contrasts, flows through valleys would be enhanced by the high pressure/low pressure contrast on the windward/leeward side of the ridge. Figures 8 and 9 show offshore flow and land breeze for a low coastal mountain. Unlike the onshore flow case with constant friction on the lee side of the mountain, a pronounced minimum in the PBL height does not occur when there is a reduction in friction on the seaward side of the mountain. This case strongly contrasts with the offshore flow case for flat topography in that there is virtually no variation in velocity seaward of the coastline. In the land breeze case, the temperature contrast reinforces the down slope flow resulting in a wind speed maximum of 9 m/s at the coast, reducing to 4 m/s at 20 km offshore.

Several important qualitative results can **be** inferred from the I-D model runs. First, the length scale for frictional and thermodynamic equilibrium *over* water is several 100's of kilometers; this is consistent with observations of wintertime cold continental **air** outbreaks over the Atlantic Ocean **along** the northeast coast of the United States. Second, in the vicinity of discontinuities, **advective** effects are *very* important. Third, the presence of even modest orography modifies the offshore flow pattern. One can anticipate that **alongshore** variations in topography are **also** important. Finally, except for certain special cases, observations made right at the coast should be, at best, only qualitatively similar to the offshore flow field.

5. SIMULATION FOR PUGET SOUND - STRAIT OF JUAN DE FUCA

A matter of primary importance is the determination of the transport mechanism of petroleum if spilled into the waters of **Puget** Sound and South-east Alaska. Since winds have a **sizeable** effect upon surface drift, direct measurements of winds over the water are being made as part of coastal assessment programs. A goal of the regional meteorological model is to extend the usefulness of these observational data sets and to enhance the understanding of the **mesoscale** atmospheric response.

We have selected three generalized meteorological flow conditions for the Puget Sound system, corresponding to typical summer and winter regimes. In the summer months, **anticyclonic** flow around a well-developed semi-permanent high pressure cell to the west of the region causes prevailing **north-west** winds offshore along the western coasts of Washington and Vancouver Island. Midwinter is characterized by a series of **cyclonic** storms with strong winds from the southwest carrying warm moist air **inland** over Western Washington. A frequent winter case is the **lull** between storms with high pressure to the east of the region giving easterly winds along the Strait of Juan de **Fuca** and relatively light winds elsewhere.

5.1 Regional Description

The area investigated is comprised of Western Washington, the southern end of Vancouver Island, and Southwest British Columbia. Major features are: the offshore ocean, **Puget Sound**, and the Straits of Juan de Fuca and Georgia (Figure 10a). This region, spans the coordinates **121°W** to **126°W** and **46°N** to **56°N**. Topographic data for the model were obtained from a master tape at the National Center for Atmospheric Research (NCAR). The **mesh is** a 5-minute of latitude-longitude grid **with** an average elevation computed for each square. The **NCAR** elevation data were smoothed in both directions with a 1-2-1 type smoother (**Shuman, 1957**). Figure **10b** presents a view of the smoothed topographic grid as seen from the southwest.

The Cascade Mountains form a north-south barrier to the east ranging from a low elevation of 916 m at **Snoqualmie** Pass to a high of 4392 m at Mt. Rainier, with an average height of 1800 m. The Olympic Mountains in the center of the region rise gradually from the south and west to 2428 m at the summit of Mt. Olympus, with an average height of 1600 m, descending rapidly to the north and east. A significant area of higher elevation to the south is the **Willapa Hills** 300-600 m high between the Columbia River and the **Chehalis** River Valley. Vancouver Island is primarily mountainous, with heights averaging 900 m, reaching 1200 m in several locations.

This topography establishes **one** main north-south low **level** passage-way extending from the Columbia River Valley through Puget Sound, and two **low** level east-west passages between the central basin and the Pacific Ocean, the Strait of Juan de Fuca and the Grays Harbor **Inlet-Chehalis** River Valley. To the northwest, Puget Sound opens out into the San Juan Islands and the Georgia Strait. The flat **land** to the east of Georgia Strait narrows eastward as the Fraser River Valley.

5.2 Data Sources

We wished to obtain a set of data which would adequately represent the regional wind field during November and December of 1976 and January of 1977. This set included routine meteorological station reports supplemented by an array of recording anemometers at strategic locations. Figure 11 and Table 2 provide station location, source and National Weather Service station symbols. Teletype data for National Weather Service Offices and Coast Guard Stations were obtained from the Ocean Services Unit of the Seattle Weather Service Forecast Office. The Weather Service Offices and ships from the northeast Pacific typically report every 6 hours. The Coast Guard Stations usually report every 3 hours, but most do not report during the night. Three MR1 Model 7092 Anemometers were set out by the authors. These yielded strip charts, which were converted to 1-hour averages and plotted every 6 hours. Data from 3 vector averaging anemometers in the Strait of Juan de Fuca were provided by Jim Holbrook as part of the Puget Sound MESA project. It should be noted that stations in Table 1 designated as 10-17 are well inland, and thus local microtopography affects the air movement at these more than at the shore stations, and are less indicative of the general flow. Station wind reports were mapped every 6 hours from 0000 Greenwich Mean Time (GMT) on November 27, 1976 to 1800 GMT on January 26, 1977. From these regional maps, examples of typical weather events were selected.

For each case selected, large-scale synoptic pressure maps centered on Western Washington were prepared from North Pacific synoptic charts. In addition objective sea level pressure analyses on the Limited Area Fine Mesh Model (LFM) grid were obtained for the region from the National Meteorological Center. Our intent is to compare the objective analyses on the 160-km mesh to the hand-drawn charts to determine if LFM input is adequate for the regional model.

Upper-air sounding data were available from **Quillayutte** (station) on the Washington coast; weather ship PAPA located at **50°N, 145°W**; SEATAC airport, south of Seattle; and Portage Bay in Seattle.

The pressure analyses have pressure given in millibars, written out on isobars to the units place and to the tenths place at stations (deleting the first two digits), e.g. 236 = 1023.6 mb. **Wind** is given on these maps as barbs (one full barb = 10 knots). On the local wind maps, direction and speed are also given at stations, e.g. 3408 = wind from true north direction 340, speed at 08 kn.

5.3 Meteorological Case Discussion

Two basic regimes describe the general **weather** characteristics of **Decembers** in **Western** Washington. As is **typical** of the latitude, a succession of frontal passages from the west, varying in number and intensity, dominates the flow patterns providing strong winds from the southwest. Between storms, high Pressure builds up near **the** area, often *in* the continental interior, bringing clear skies and relatively low winds lasting for several days to a week or more. The fall and winter of **1976** were unusual in that a persistently recurring ridge of high pressure over the northeastern Pacific at 500 mb, frequently extending **almost** to the pole, allowed only an occasional weakened frontal passage through the area. Surface high pressure associated with the 500-mb pattern, but displaced eastward over the continent, dominated the Puget Sound Basin.

A good example of this situation is 0000 GMT on December 1, 1976. For several days prior to and succeeding this time, high pressure prevailed over southeastern British Columbia, extending north and south over **the** interior plateau (Figure 12). In the absence **of** topography, widely spaced isobars would suggest a weak **flow** outward from the high pressure center westward over the area. However, the local wind shown in Figure **13** reveals a complex pattern with easterly winds at the coast and calm or light northerly winds in the Puget Sound. A very **interest-**ing feature is seen in the Strait of Juan de **Fuca**. In sharp contrast to the weak and variable winds elsewhere on the inland waters, there is a **strong** flow out the Strait, reaching 20 kn at Cape Flattery. This isolated jet was reported on by Reed (1931) but is not specifically mentioned in more recent literature. Associated with these low level wind vectors are temperature soundings over the area revealing a strongly stratified regime throughout the planetary boundary layer. The SEATAC sounding for November 30, 1976 at 1610 GMT is shown in Figure 14. Lines of constant potential temperature are **also** shown indicating stable stratification throughout the boundary layer.

On the objective analyses from the National Meteorological Center, the absence of horizontal air flow seen at 850 mb in Figure 15 for December 1, 0000 GMT **contrasts with the surface pattern (Figure 16)** which shows a **light pressure gradient east-west through the region** in agreement with the **hand-drawn map**. The spacing on the surface **LFM** map is 1 mb, approximately **equivalent** to the 10-geopotential meter spacing of the **850-mb** LFM map. The **decoupling of the 850 mb and surface layer** is consistent with the strong vertical stratification observed at **SEATAC**. Stability restricts the flow to regions below the mountain tops where the air is accelerated along the **east-west** pressure gradient out through the Strait of Juan de Fuca and west through the **Cowlitz** Valley south of the Olympic Mountains. The winds can be explained as stronger in the Strait than along the southern Washington coast **because** the down gradient acceleration is uninhibited by surface friction. Another curious feature is that the winds in Puget Sound proper flow south in the opposite direction to an inferred surface **geostrophic** wind. A second example of winds under the high pressure regime is seen in Figures 17 and 18, where high pressure has built up rather rapidly between frontal passages. The local stations again reflect the widely spaced isobars with easterly winds on the coast, calm in the Sound and acceleration along the Strait of Juan de Fuca.

Figure 19 shows the wind pattern generated by the model which corresponds to the December 1, 1976 case. While the boundary layer is not well mixed as assumed in section 2, we considered that we could simulate the forced channeling for the east wind case by assuming a very shallow PBL in the model capped by very strong stability. Input parameters are summarized in Table 3. The model was initialized by a geostrophic wind of 4.8 ins-i from 144° and a low PBL height of 0.5 km as representative of stable conditions throughout the lower troposphere. The major features are: light winds in the central basin, weak easterly flow along the coast, and accelerating easterly flow down gradient through the Strait of Juan de Fuca, similar to Figures 13 and 17. As the flow in all channels is out of the Puget Sound Basin, this case could not be run to steady state. In the prototype the outflowing air is replaced by subsidence associated with the synoptic high pressure. Subsidence is not included in the model to balance the falling PBL height; Figure 19 is the model-estimated wind field when the interior PBL height reached 400 m after 4 hours and was falling at a constant velocity. To increase the resolution in the main area of interest, the Strait of Juan de Fuca, the grid length was reduced to one-half of its previous value in the north-south direction, while the domain was also reduced to see if the model could be sectionalized (Figure 20). Good agreement is obtained in the Straits. Contrary to the inferred flow from observations, at the east end of the Strait a more geostrophic flow is allowed by not resolving the southern end of Puget Sound.

The front that approached the coast at 0000 GMT, December 8, 1976 (Figure 21) turned into a cold front of respectable energy as the high retreated far to the south. This case of even isobars and southwesterly **geostrophic** flow is a good example of the typical situation before the passage of a cold front. From the **local** wind vectors (Figure 22), one first notices that the flow is channeled **by** the Olympic and Cascade Mountains. Winds over Puget Sound **are stronger** and more southerly than offshore. A region of light winds is evident **in** the lee of the Olympic Mountains. There is also general steering of the flow **along** the axis of Georgia Strait, more than a 90° deflection from the geostrophic wind. The December 7 1605 GMT temperature sounding at SEATAC shows a relatively moist, deep, well-mixed PBL with near-neutral stability (Figure 23). This is illustrated further by the fact that the **850-mb** flow is very similar to the surface flow on the LFM maps (see Figures 24 and 25). The hand-drawn and LFM surface maps agree well. Figures 26 and 27 for 0000 GMT, December 15, show an additional **example of strong winds from the southwest**.

The corresponding storm situation of December 8, 1976, is simulated by a model run in Figures 28 and 29 for a PBL height of 1800 m and 900 m, respectively. Geostrophic wind is 14.7 m/s^{-1} from 251° . The overall wind pattern for the observed PBL height (1800 m) is much smoother than that suggested by observations. The lower height, however, shows the approximate amount of detail. A relative eddy has formed at the east end of the Strait of Juan de Fuca near Port Angeles to various degrees in both simulations. The PBL height deviations show a gentle rise over the windward side of the mountains with a pronounced lee wave trough on the downwind side of the Olympics and Vancouver Island. With a low inversion height, increased winds flow through the low point in the mountains of Vancouver Island and spill out over the inland waters. Observed winds in the east end of the Strait of Juan de Fuca are less intense and more westerly than either model run suggests. It may be that the position of the eddy and the magnitude of the pressure gradient that develops along the axis of the Strait of Juan de Fuca are very sensitive to the volume of air channeled through Puget Sound, which depends in turn on the orientation of the offshore flow. Inflow along the southern boundary is not handled satisfactorily by arbitrary specification of inversion height, especially at the land-water interface. However, this does not appear to unduly influence the flow in the central basin.

In the previous section it was noted that inertia plays a dominant role in **mesoscale** circulations. In contrasting the two **model** runs, the main differences are between allowing the flow to go over the mountain or forcing it around the mountain. Since observations resemble more the case with a lower inversion, perhaps the effective cross-sectional height of the mountains is higher than the model-assumed average elevations; the light stable stratification of the PBL shown in the SEATAC sounding may contribute to increased channeling.

The front depicted in Figure 17 was the weakest of four crossing the region in December 1976. For a day following the December 22 front and a day following the December 8 front, a cell of high pressure existed off the coast of Oregon and Northern California which brought strong northwesterly winds through Washington as part of an anticyclonic circulation. Except for temperature effects, this pattern **is** typical of summertime conditions in the region. The hand-drawn pressure map of December **23**, 1976, 1800 GMT shows a relatively uniform pressure gradient from offshore inland to Vancouver, B.C. (Figure 30). The local anemometers (Figure 31) reveal the effect of topography on a northwesterly **geostrophic** wind. Strong **channeling** is indicated in the Strait of Juan de Fuca with variable winds in the lee of the Olympic Mountains. It is interesting that for this case and for December 9, 1976, 1200 GMT (Figures 32 and 33), there is a southerly flow in the lower **Puget** Sound in the lee of the Olympics, but only on the surface. Figure 34 shows the December 9, 1400 GMT, **McChord** AFB wind sounding and the **Quillayutte** temperature sounding. The **LFM** maps (Figures 35 and 36) concur with the hand analysis in showing a northwesterly **geostrophic** flow.

Figure 37 shows the model velocity **field** for northwest winds. Channeling is indicated in the Strait of **Juan de Fuca and** especially in the Strait of Georgia. Height deviations are less intense than for the southwest wind **case**, although the velocity field indicates that the lee **wave** eddy is still a major feature. A southerly tendency is indicated in the lower **Puget** Sound trough where the flow is parallel to the pressure gradient **below** the ridge crests.

In contrasting the wind and height **fields** for NW and SW winds, northwest winds tend to flow fairly closely to the orientation of the ridge line. Southwest winds funnel the flow into Puget Sound, but farther north inertia carries the major **volume** flux (velocity multiplied by PBL depth) across topographic contours through the **low** points in the ridge crest. This **cross-contour** flow induces a **major local response in the height** field and eddies.

6. ACKNOWLEDGEMENTS

This study **was** supported jointly by the **Puget** Sound Marine Ecosystems Analysis (MESA) Project and the Outer Continental Shelf Environmental Assessment Program (**OCSEAP**) to assist in providing wind fields for oil spill **trajectory** calculations, and the Marine Services Program at PMEL in support of National Weather **Service** marine prediction along the west coast and Gulf of Alaska.

We wish to thank Robert Anderson and his colleagues at the Seattle National Weather Service Forecast Office for their collaboration in the field program and in compiling the routine observation data sets.

7. REFERENCES

- Brown, R. A. (1974): A **simple** momentum integral model. J. Geophys. Res. 79:4076-4079.
- Keyser, D., and Anthes, R. (1977): The applicability of a mixed-layer model of the planetary boundary layer to real-data forecasting. Mon. Wea. Rev. 105:1351-1371.
- Lavoie, R. (1972): A **mesoscale** numerical model of lake-effect storms. J. Atmos. Sci. 29:1025-1040.
- Lavoie, R. (1974): A numerical model of tradewind weather on **Oahu**. Mon. Wea. Rev. 102:630-637.
- Ogura, Y., and N. W. Phillips (1962): Scale analysis of deep and shallow **convection in the** atmosphere. J. Atmos. Sci. 19:173-179.
- Reed, J. (1931): Gap winds of the Strait of Juan de **Fuca**. Mon. Wea. Rev. 59:373-376.
- Stun, R. B. (1976): Mixed-layer depth model based upon turbulent energetic. J. Atmos. Sci. 33:1268-1278.

DERIVATION OF BOUNDARY LAYER EQUATIONS

We shall write the equations of motion for deviation from a steady reference state. If the reference state changes only very **little with** height, it is possible to use the **Boussinesq** approximation, but with potential temperature as the thermal variable (**Ogura** and Phillips, 1962).

The momentum equation is:

$$\frac{\partial \vec{v}}{\partial t} + \vec{v} \cdot \nabla \vec{v} = w \frac{\partial \vec{v}}{\partial z} + f \vec{k} \times \vec{v} + c_p \theta_0 \nabla \pi = - \frac{\partial}{\partial z} (\overline{\vec{v}' w'}) \quad (A1)$$

where

$$\pi \equiv \left(\frac{p}{p_0} \right)^\chi, \quad \chi = R/c_p.$$

The hydrostatic equation is:

$$c_p \theta \frac{\partial \pi}{\partial z} = -g. \quad (A2)$$

The equation of continuity is:

$$\nabla \cdot \vec{v} + \frac{\partial w}{\partial z} = 0. \quad (A3)$$

The first law of thermodynamics is approximated by:

$$\frac{\partial \theta}{\partial t} + \vec{v} \cdot \nabla \theta + w \frac{\partial \theta}{\partial z} = - \frac{\partial}{\partial z} (\overline{w' \theta'}). \quad (A4)$$

In these equations \vec{v} is Reynolds' averaged horizontal velocity vector, \vec{v}' is the deviation velocity, θ is potential temperature, and θ_0 is the potential temperature of the reference state (constant). The other terms are defined in the usual meteorological sense.

We simplify the hydrostatic equation (A2) in the following way:

$$c_p \frac{\partial \pi}{\partial z} = - \frac{g}{\theta} \approx -g \frac{1}{\theta_0} \left(1 - \frac{\theta''}{\theta_0} \right),$$

where $\theta'' = \theta - \theta_0$.

If we define π_0 such that

$$c_p \frac{\partial \pi_0}{\partial z} = -\frac{g}{\theta_0}$$

then

$$c_p \frac{\partial \pi''}{\partial z} = \frac{g}{\theta_0} \frac{\theta''}{\theta_0}, \text{ where } \pi'' = \pi - \pi_0.$$

Since π_0 is a function of z only, we can rewrite Eqn. (A1):

$$\frac{\partial \vec{v}}{\partial t} + \vec{v} \cdot \nabla \vec{v} + w \frac{\partial \vec{v}}{\partial z} + f \vec{k} \times \vec{v} + c_p \theta_0 \nabla \pi'' = -\frac{\partial}{\partial z} (\overline{\vec{v}'w'}) \quad (\text{A6})$$

We shall use equations (A3), (A4), (A5), and (A6) for describing the flow field in the well-mixed layer.

We now integrate (A4) and (A6) through the mixed layer. The basic equations then become:

$$\frac{\partial \vec{v}}{\partial t} + \vec{v} \cdot \nabla \vec{v} + f \vec{k} \times \vec{v} + \frac{c_p \theta_0}{h-D} \int_0^h \nabla \pi'' dz = -(\overline{\vec{v}'w'}_h - \overline{\vec{v}'w'}_s) / (h-D) \quad (\text{A7})$$

$$\frac{\partial \theta}{\partial t} + \vec{v} \cdot \nabla \theta = -(\overline{w'\theta'}_h - \overline{w'\theta'}_s) / (h-D) \quad (\text{A8})$$

In addition, the mass continuity equation, by definition, can be written:

$$\frac{\partial h}{\partial t} + \nabla \cdot (h-D) \vec{v} = E, \quad (\text{A9})$$

where E is the net entrainment rate at which the well-mixed layer gains mass from the free atmosphere.

Using hydrostatic equation, we evaluate the vertically integrated pressure gradient force:

$$-\frac{c_p \theta_0}{(h-D)} \int_0^h \nabla \pi'' = -c_p \theta_0 \nabla \pi''_H + \frac{g}{\theta_0} (H-h) \nabla \theta''_H - \frac{g}{\theta_0} (\theta''_h - \theta''_s) \nabla h + \frac{g}{\theta_0} \frac{1}{2} (h-D) \nabla \theta'' \quad (\text{A10})$$

where subscript H denotes the top of the model atmosphere.

For the convenience of finite **differencing**, Eqn. (A8) is written in a flux form:

$$\frac{\partial}{\partial t} (h-D)\theta + \nabla \cdot (h-D)\vec{v}\theta - \theta E = -(\overline{w'\theta'})_h + (\overline{w'\theta'})_s \quad (\text{A11})$$

In deriving the equation, Eqn. (A9) was used.

Integrating Eqns. (A1) and (A4) across the **jump between the PBL and inversion layer** using **Leibnitz' rule**, we obtain relations:

$$\overline{(\vec{v}'w')}_{h^-} = -E\Delta\vec{v} \quad (\text{A12})$$

$$\overline{(w'\theta')}_{h^-} = -E\Delta\theta \quad (\text{A13})$$

where $\Delta\vec{v} = \vec{v}_+ - \vec{v}_-$ and $\Delta\theta = \theta_+ - \theta_-$.

Equations (A7), (A9), and (A11) with equations (A10), (A12), and (A13) form a closed set of equations, if the entrainment rate can be parameterized in terms of the mixed layer variables.

FIGURE CAPTIONS

- Figure 1. Regions of anomalous winds as reported by vessels operating in Alaskan waters.
- Figure 2. Model-defined parameters of height, velocity and potential temperature. In application $\gamma=0$ and $\theta_H=\theta_+$.
- Figure 3.** Staggered mesh for primary variables.
- Figure 4a. Onshore flow with flat coastline.
- Figure 4b. Onshore flow with flat coastline with acceleration terms set to zero.
- Figure 4c. Sea breeze circulation with a flat coastline.
- Figure 5a. Offshore wind with flat coastline.
- Figure 5b. Land breeze circulation with **flat** coastline.
- Figure 6a. Onshore flow with coastal mountain; offshore PBL =500 m.
- Figure 6b. Onshore flow with coastal mountain; offshore PBL = 900 m.
- Figure **6c.** Onshore flow with coastal mountain; offshore PBL = 1500 m.
- Figure 7. Sea breeze circulation with coastal mountain.
- Figure 8. Offshore **flow** with coastal mountain.
- Figure 9. Land breeze **with** coastal mountain.
- Figure 10a. Location map for the **Puget** Sound Basin.
- Figure **10b.** Topographic grid used in the computations as viewed from the **south-west**.
- Figure **11.** Location map for anemometer stations collected for December 1976 - January 1977.
- Figure **12.** Sea level pressure analysis 1 DEC 76, **0000GMT.**
- Figure 13. Local wind observations 1 DEC 76, **0000GMT.**
- Figure 14. Atmospheric sounding for SEATAC 30 NOV 76, 1610GMT.
- Figure 15. Objective analysis **of 850-mb** heights **1** DEC 76, **0000GMT.**
- Figure 16. Objective analysis of sea level pressure 1 DEC 76, **0000GMT.**

FIGURE CAPTIONS (continued)

- Figure 17. Second **example** of high pressure to the northeast of Puget Sound, **21 DEC 76, 1800GMT.**
- Figure 18. Local wind observations for **pressure** field shown in Figure 17.
- Figure 19. Model run for east wind case.
- Figure 20. Model run for east wind case **with** increased north-south resolution.
- Figure 21. Sea level pressure chart 8 DEC 76, **0000GMT.**
- Figure 22. Local wind observations 8 DEC 76, **0000GMT.**
- Figure **23.** **SEATAC** sounding 7 DEC 76, **1605GMT.**
- Figure 24. Objective analysis **of 850-mb** heights 8 DEC 76, **0000GMT.**
- Figure 25. Objective analysis of sea level pressure, 8 DEC 76, **0000GMT.**
- Figure 26. Second example of strong onshore flow from southwest, 15 DEC 76, **1800GMT.**
- Figure 27. Local wind observations for Figure 26.
- Figure 28. Model winds for southwest flow with offshore PBL height of 1800 m.
- Figure 29. Model winds for southwest flow with offshore PBL height of 900m.
- Figure 30. Sea level pressure chart, 23 DEC 76, **0800GMT.**
- Figure 31. Local wind observations, 23 DEC 76, **1800GMT.**
- Figure 32. Sea level pressure chart 9 DEC 76, **1200GMT.**
- Figure 33. Local wind observations 9 DEC 76, **1200GMT.**
- Figure 34. Temperature sounding at **Quillayute** (Washington coast) and McChord AFB (**Puget** Sound) for 1200 and **1400GMT**, 9 DEC 76.
- Figure 35. Objective analysis **of 850-mb** heights, 9 DEC 76, **1200GMT.**
- Figure 36. Objective **analysis of sea level** pressure, 9 DEC 76, **1200GMT.**
- Figure 37. Model winds for northwest flow.

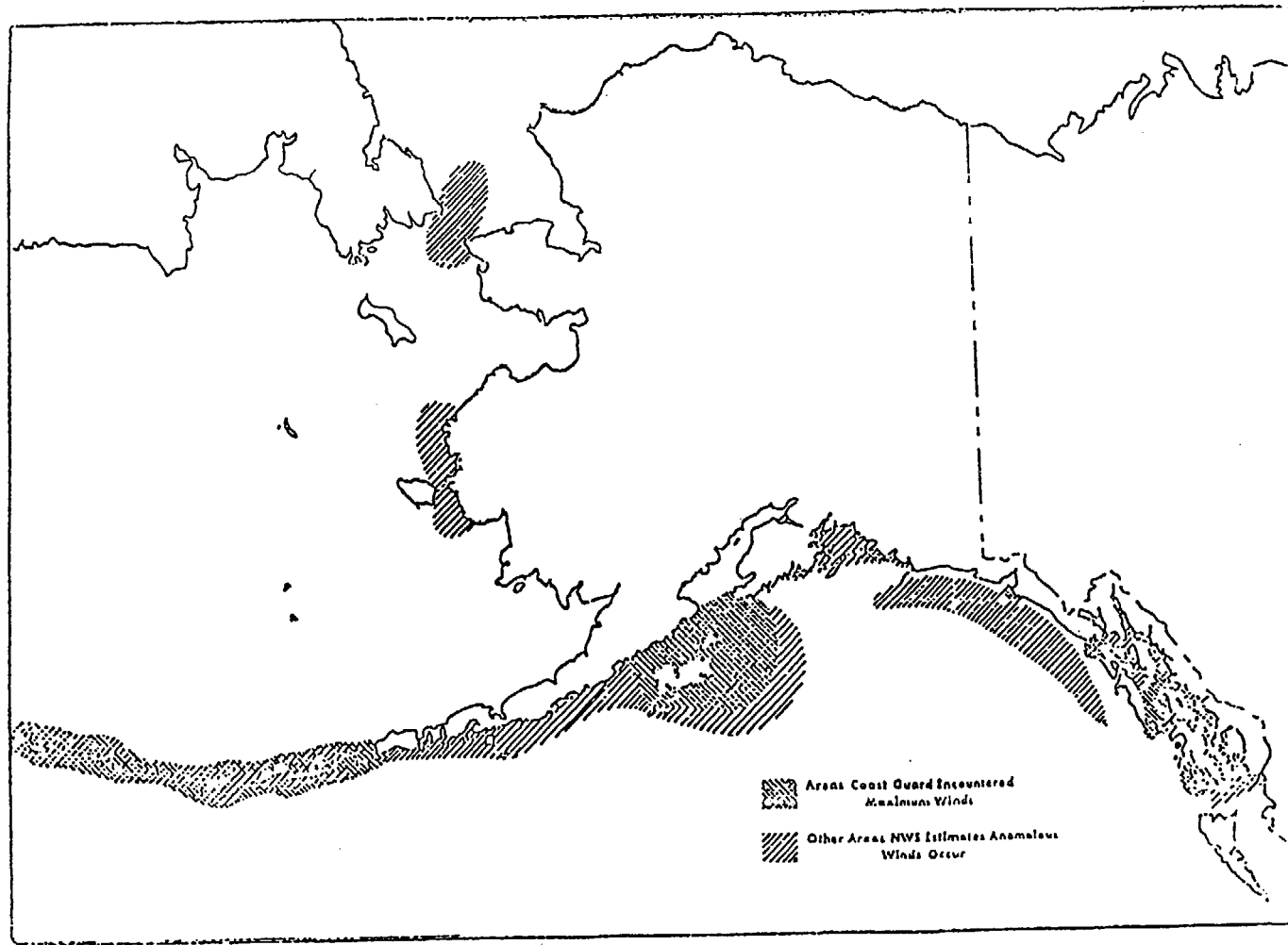


Figure 1.

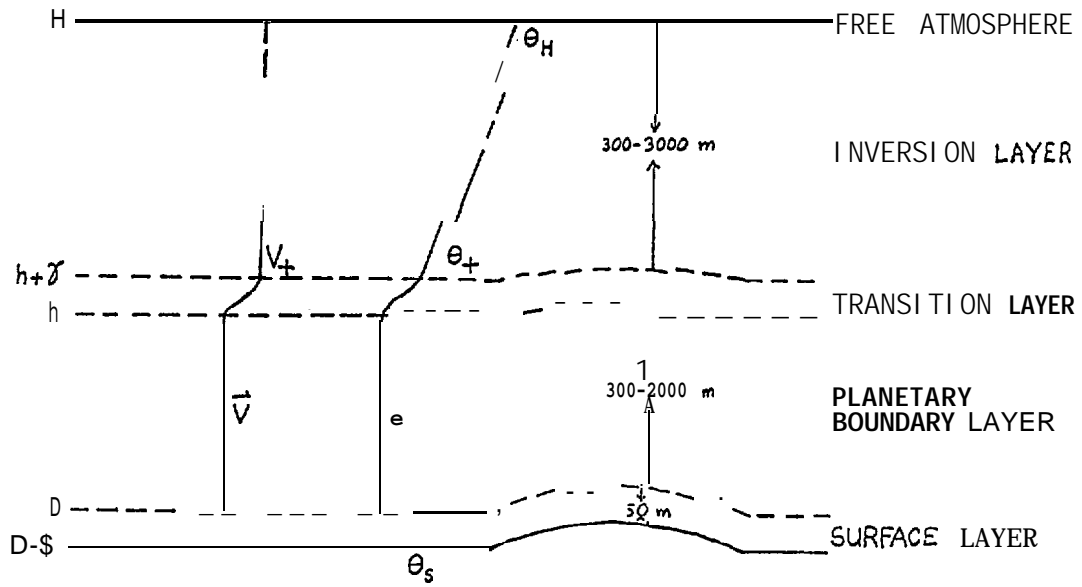


Figure 2.

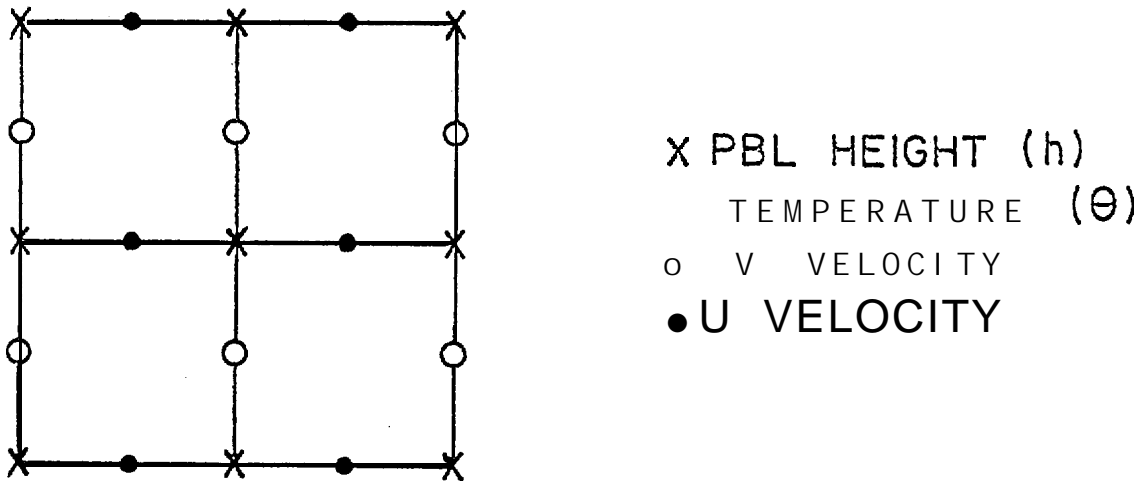


Figure 3.

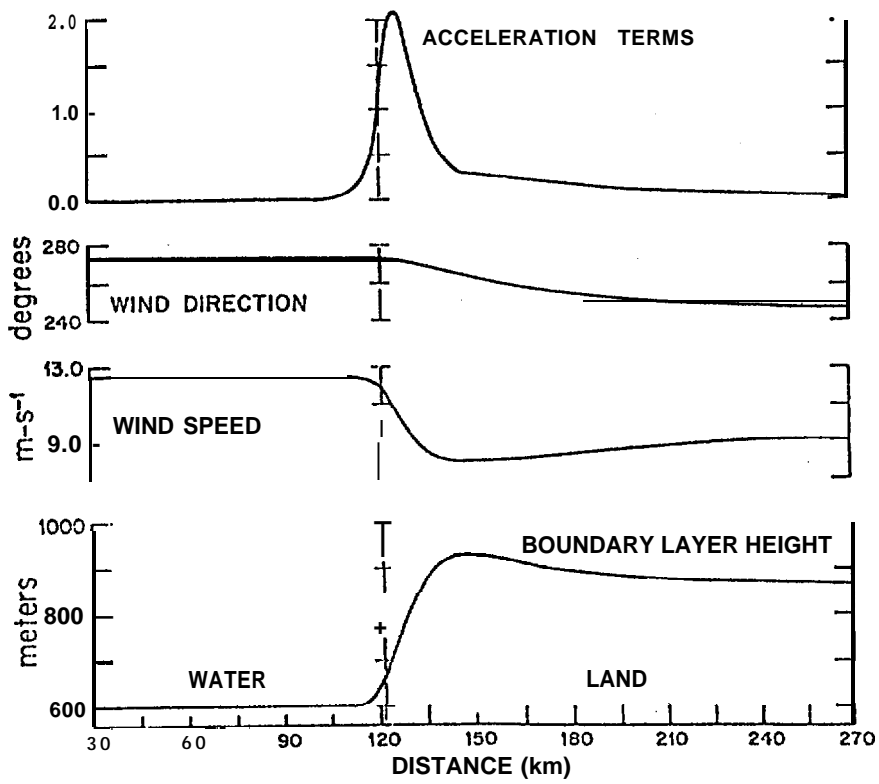


Figure 4a.

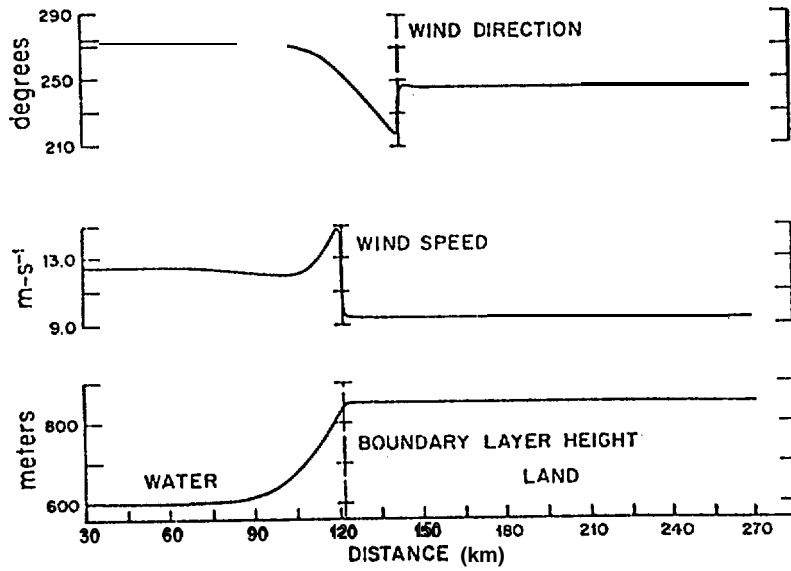


Figure 4b.

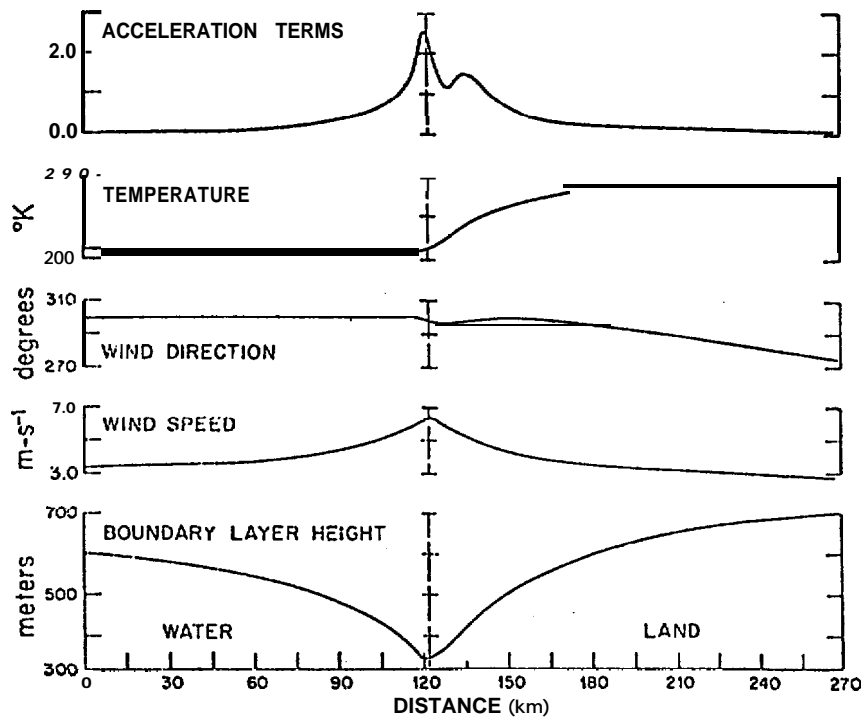


Figure 4c.

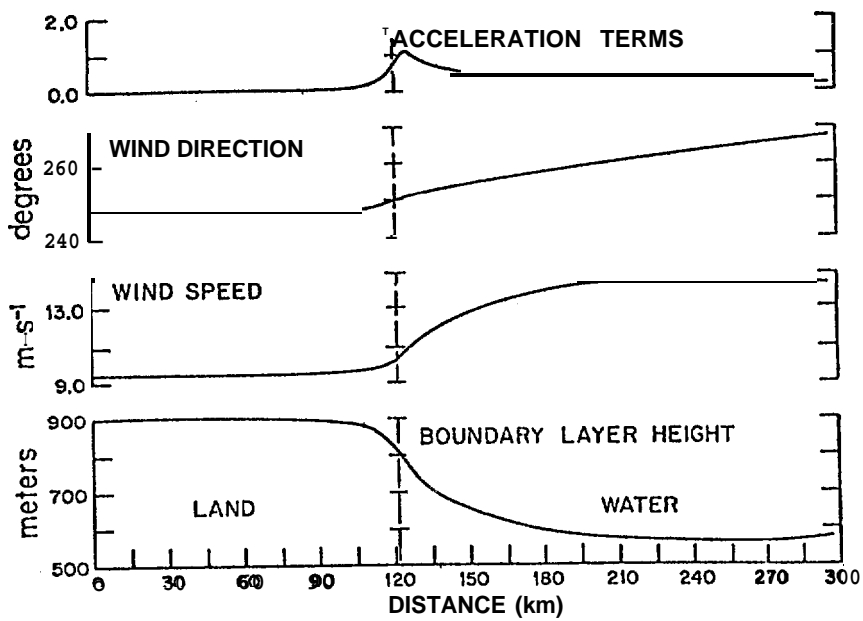


Figure 5a.

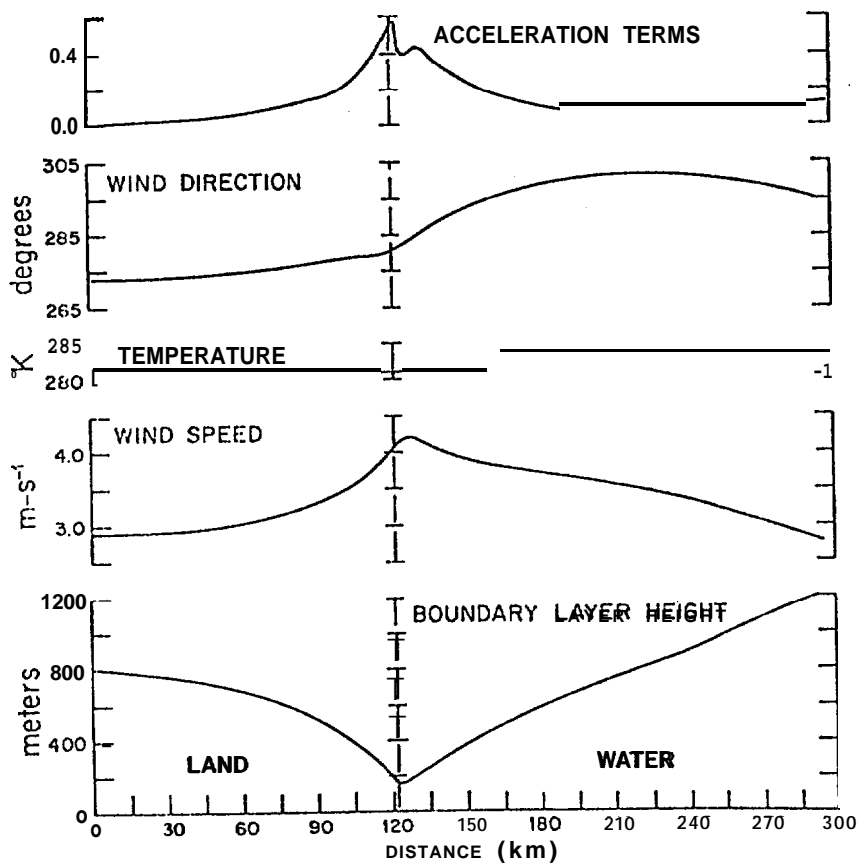


Figure 5b.

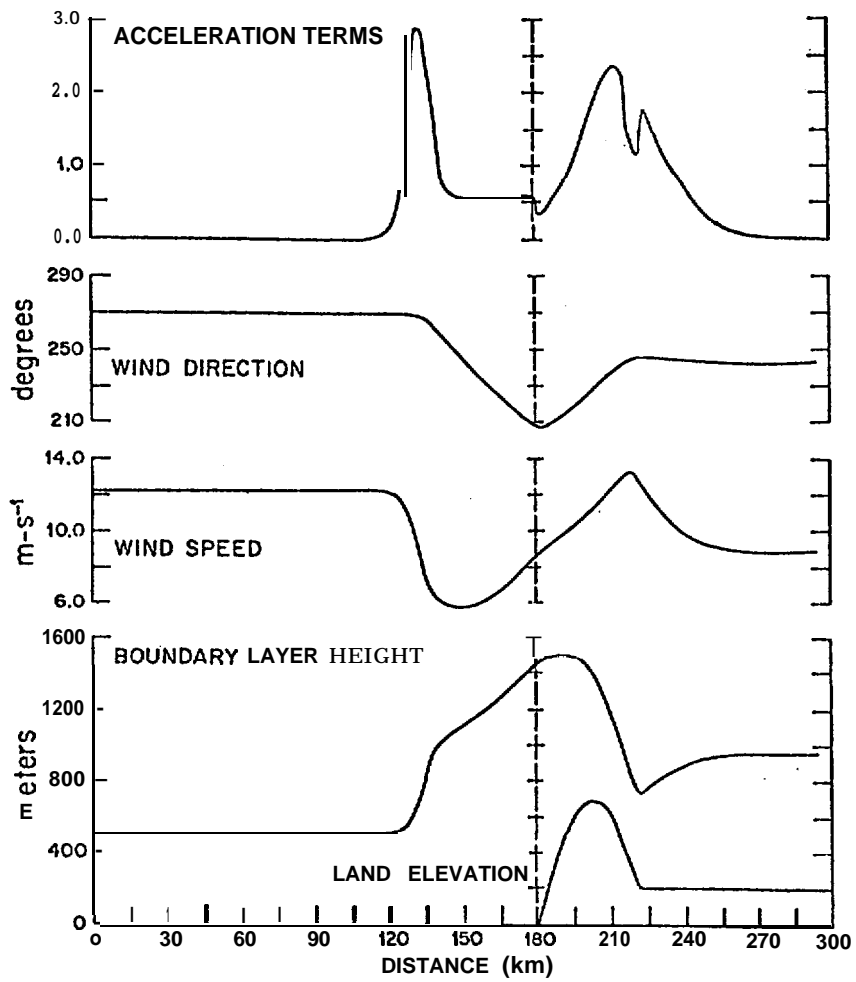


Figure 6a.

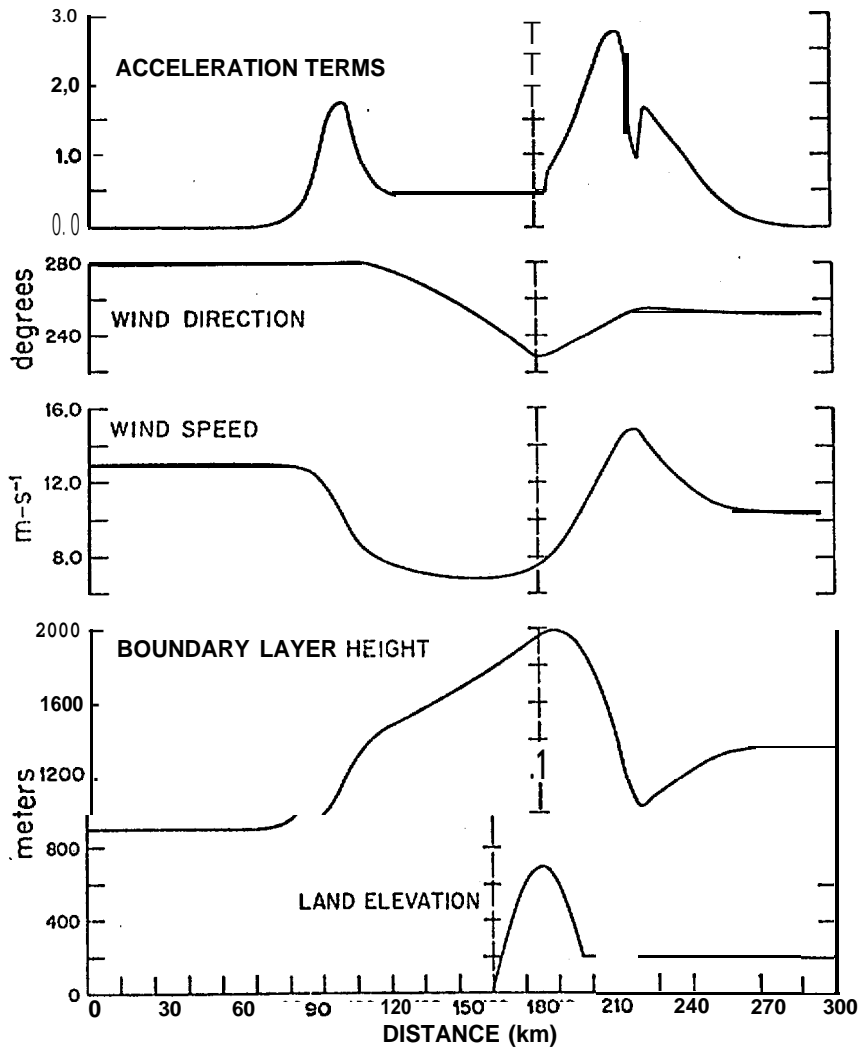


Figure 6b.

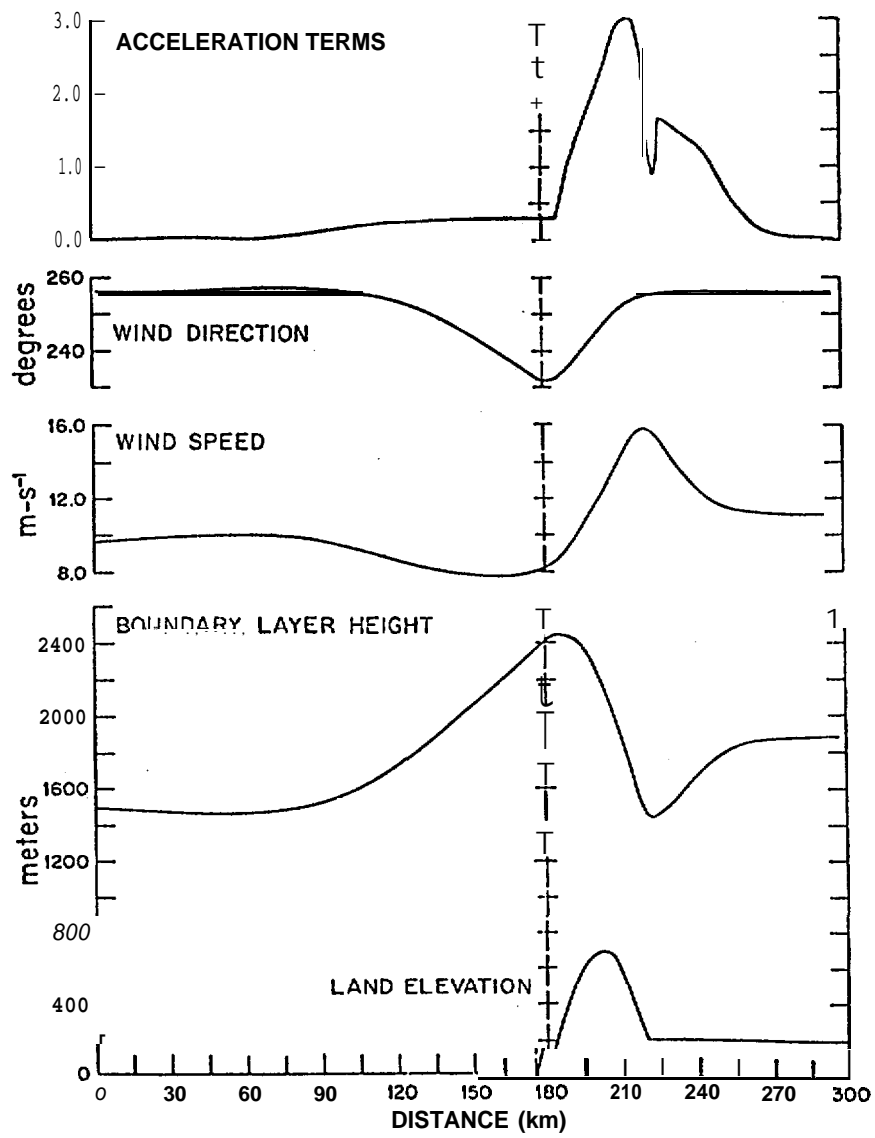


Figure 6c.

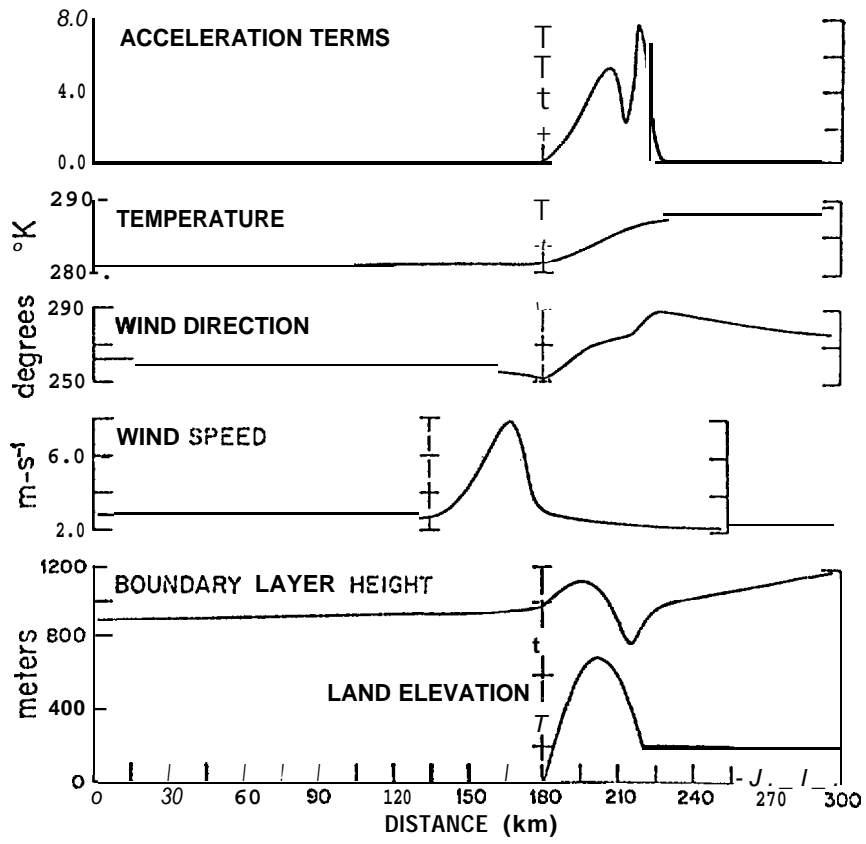


Figure 7.

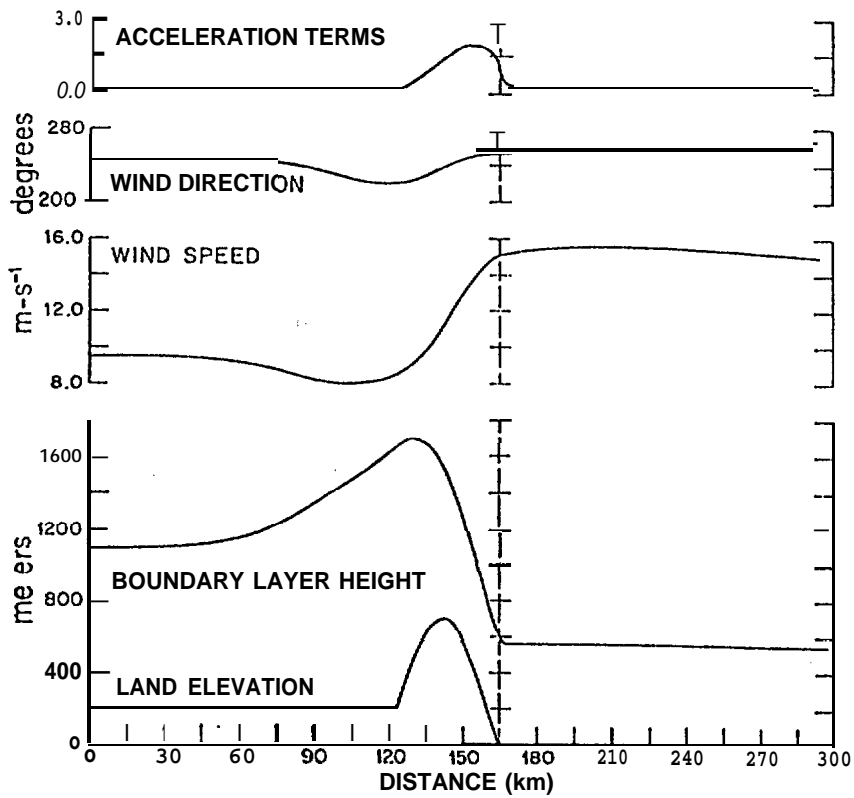


Figure 8.

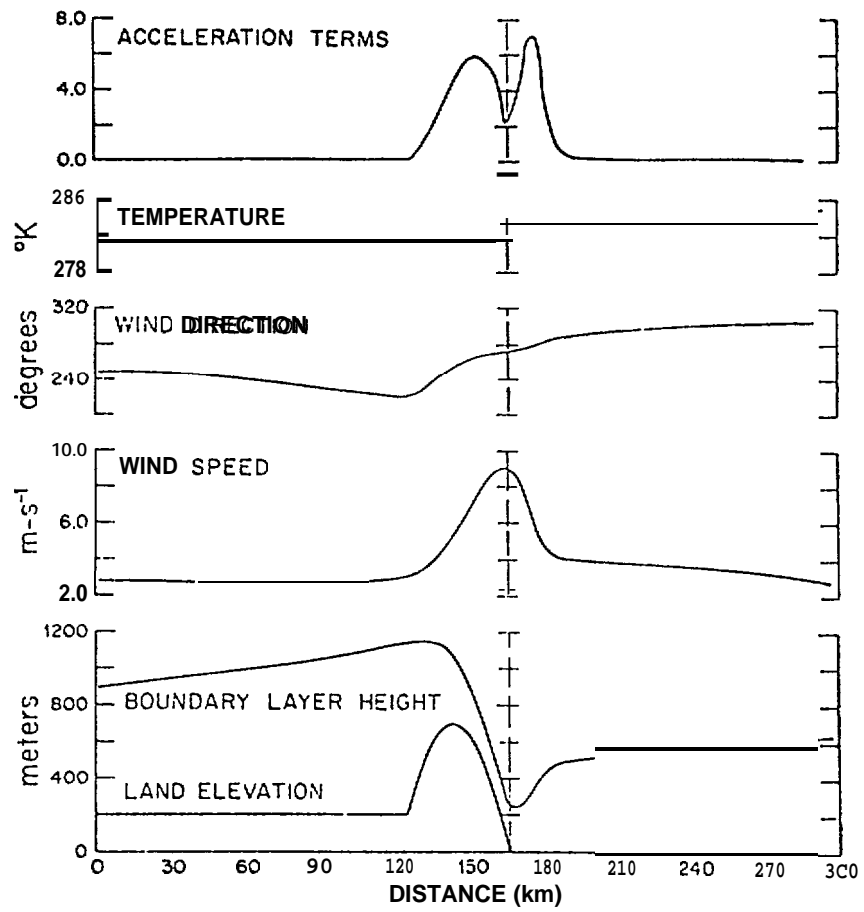


Figure 9.

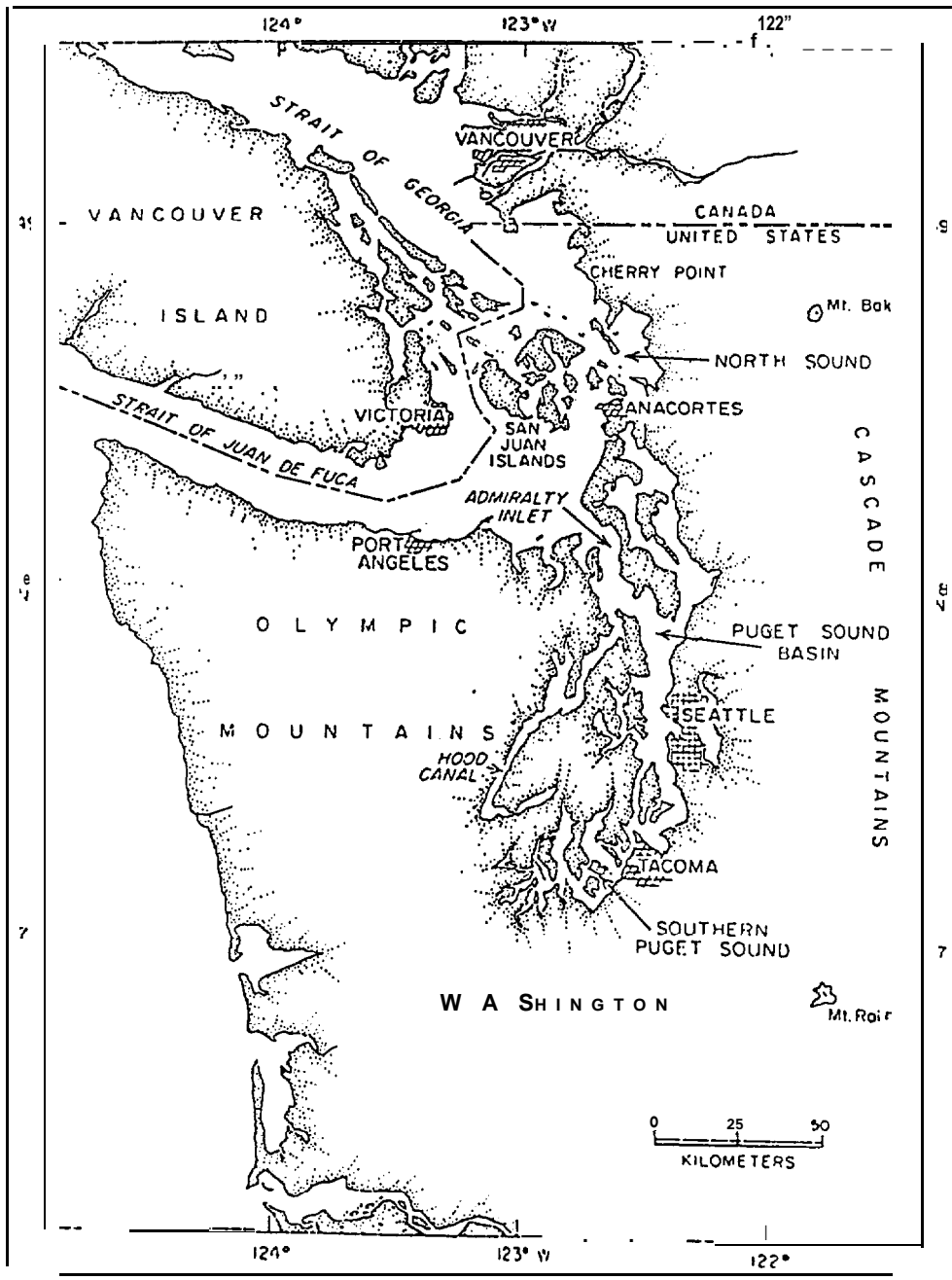


Figure 10a.

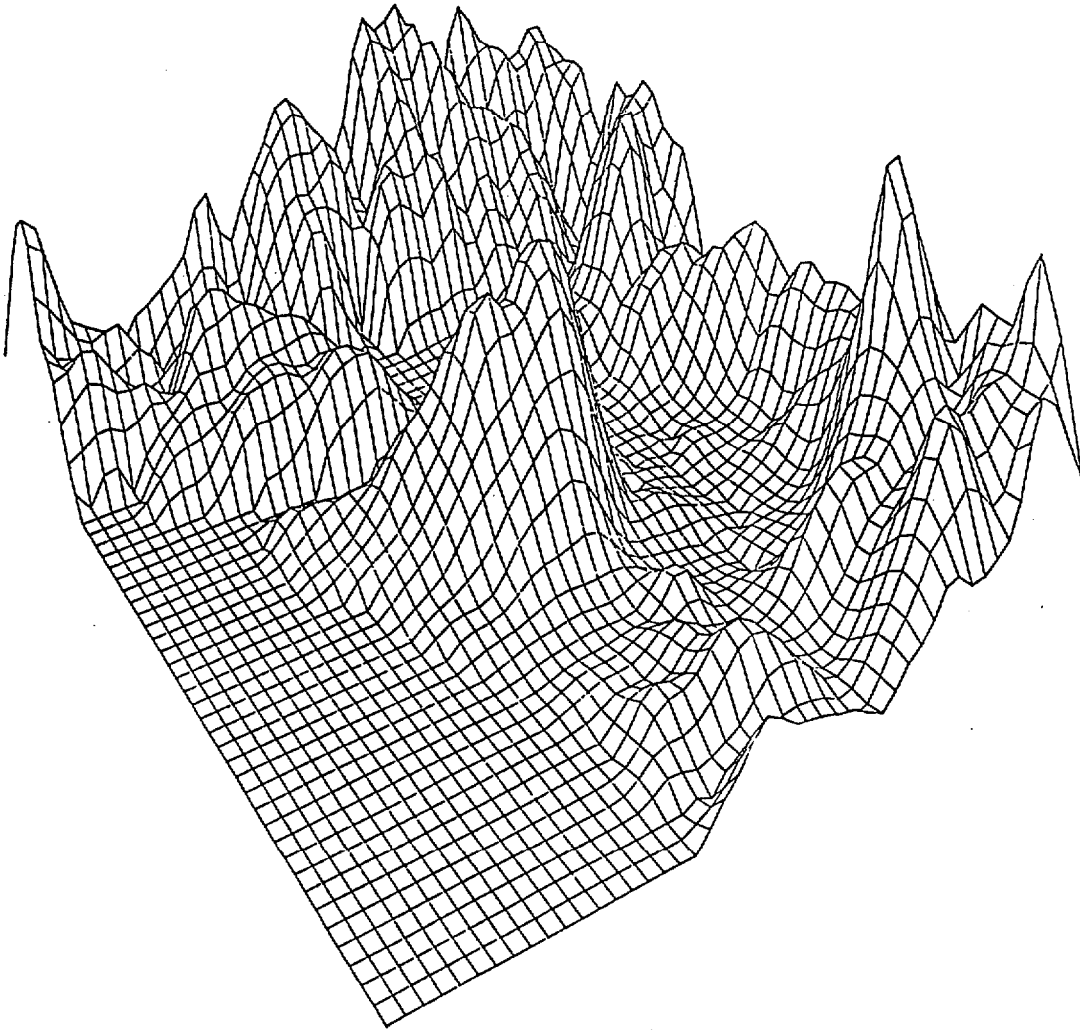


Figure 10b.

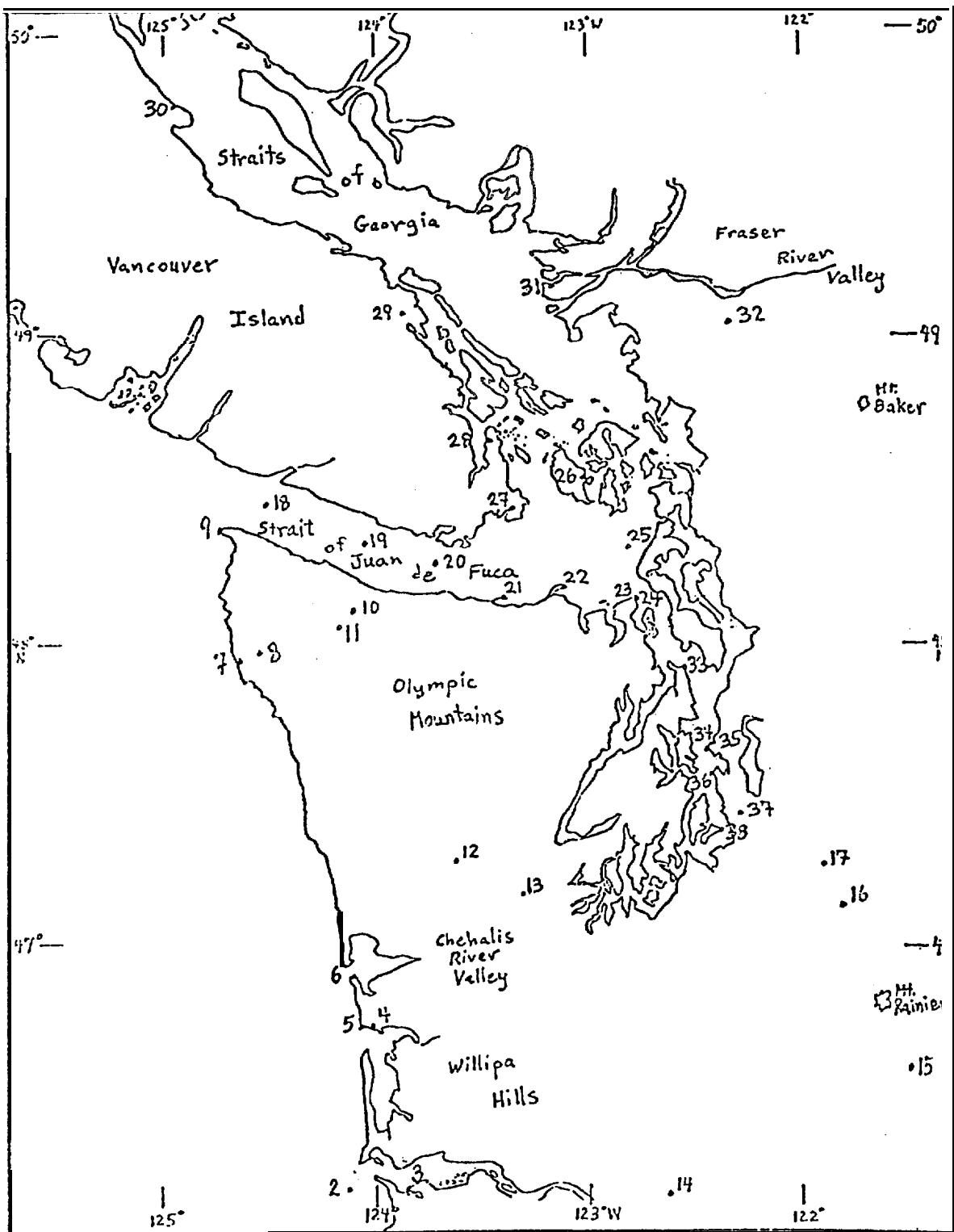


Figure 11.

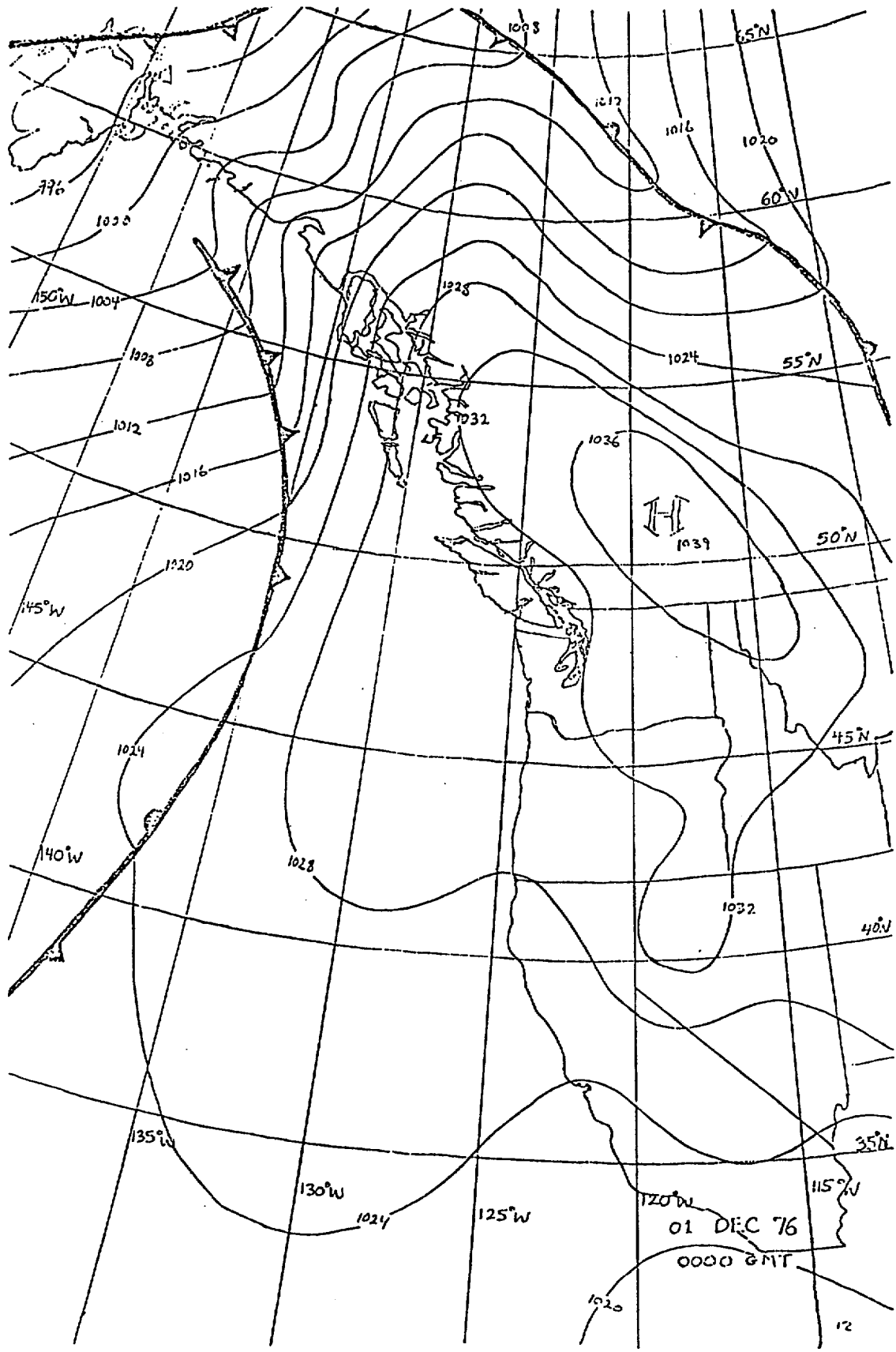


Figure 12.

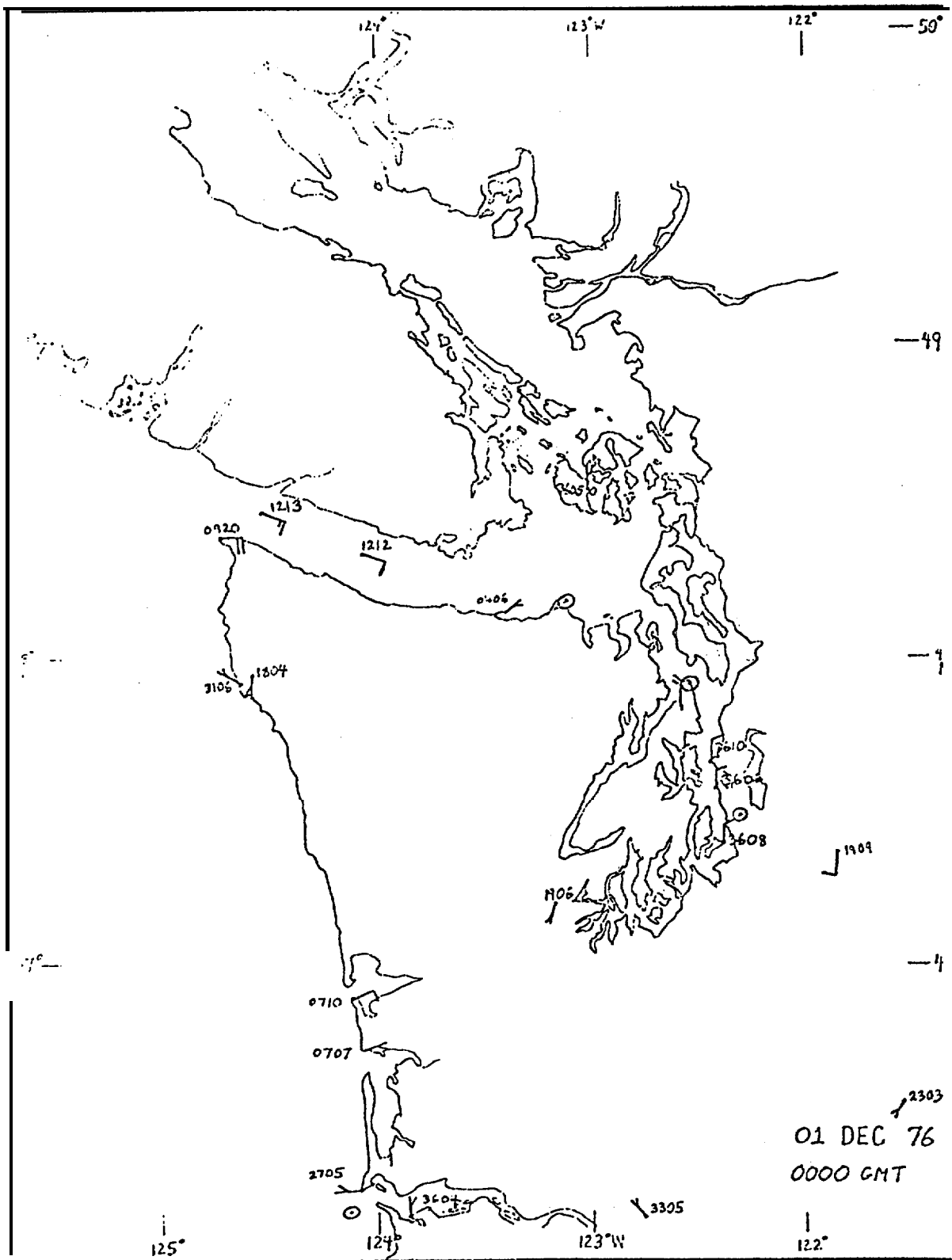


Figure 13.

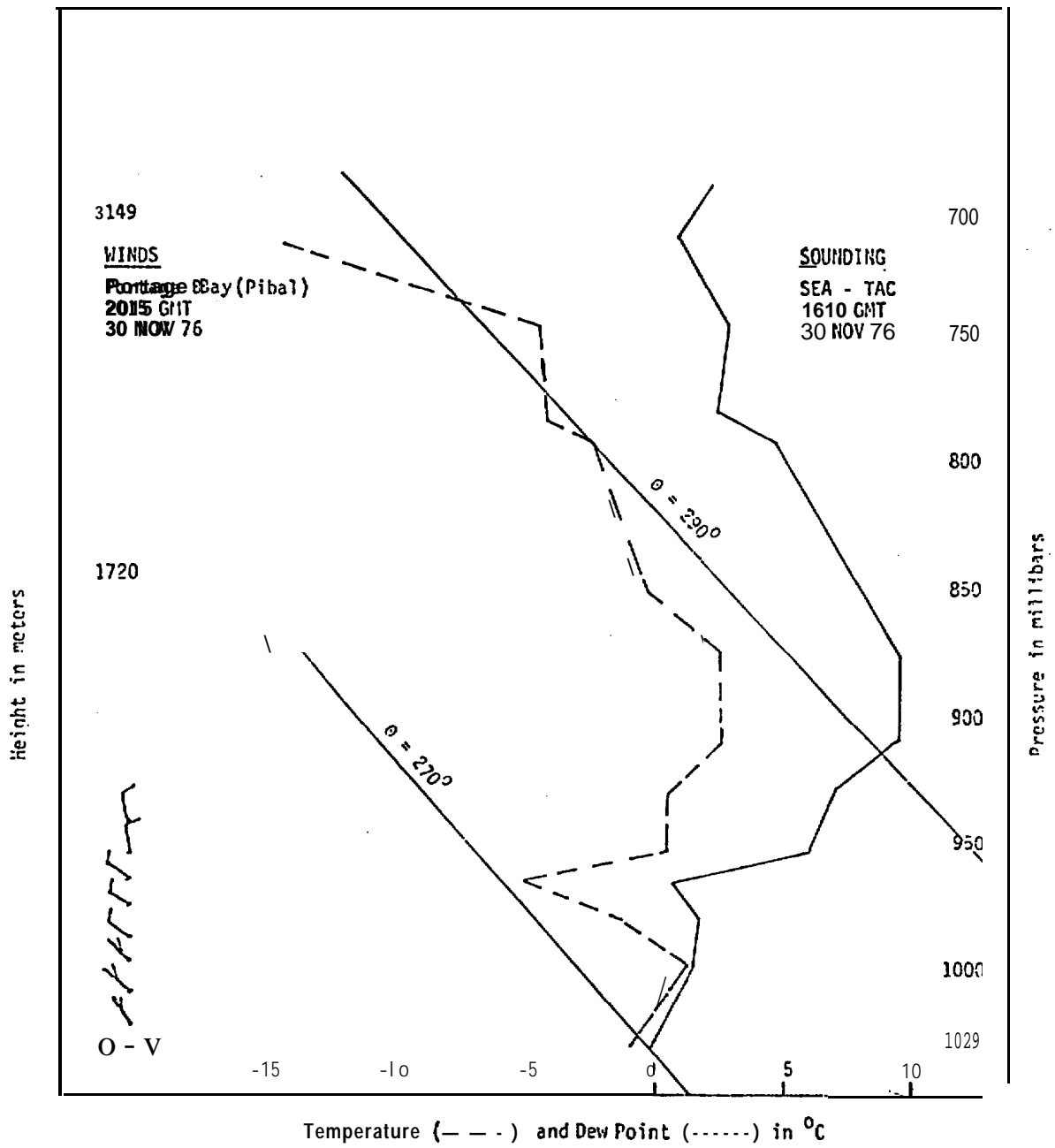


Figure 14.

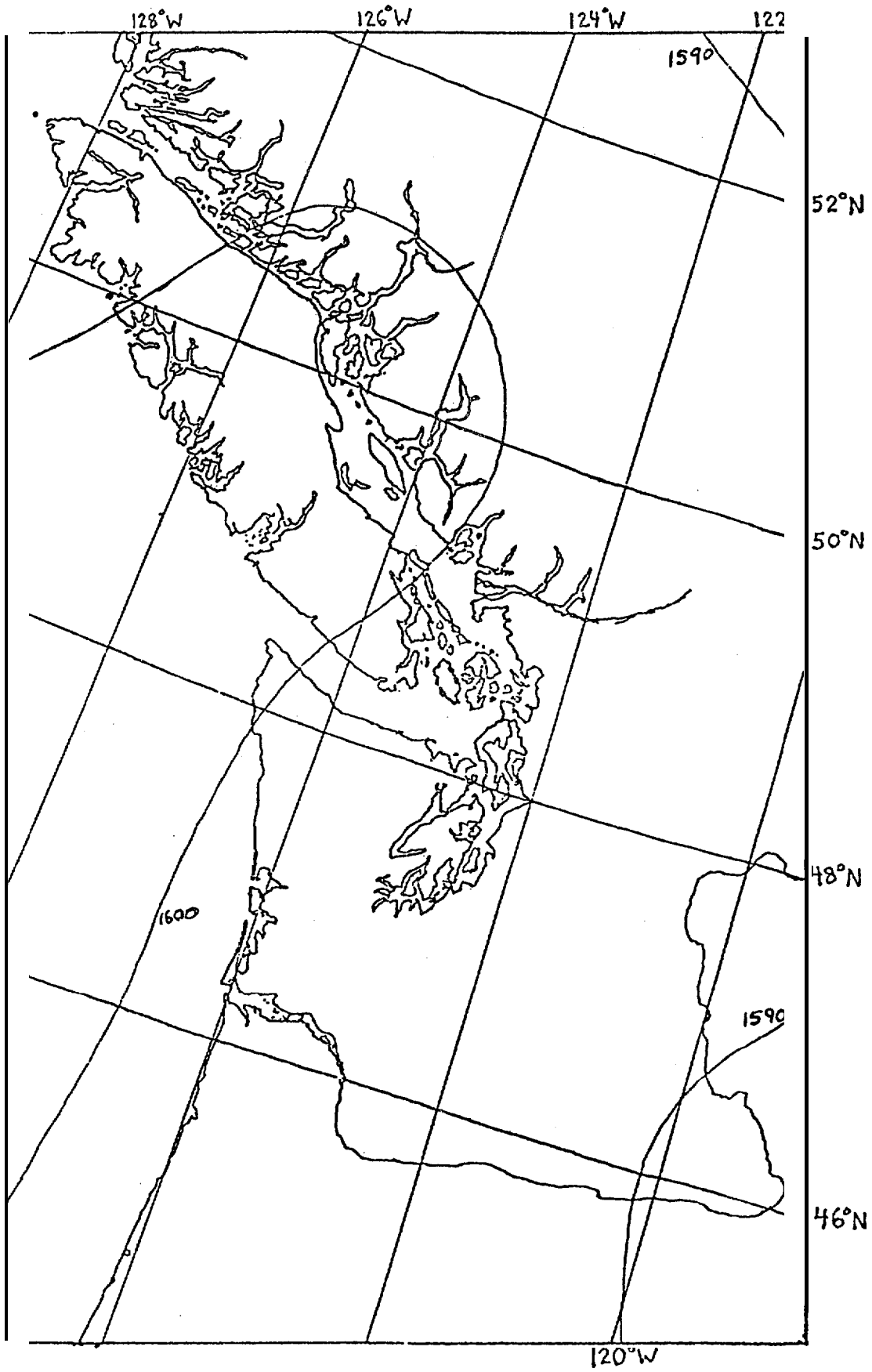


Figure 15.

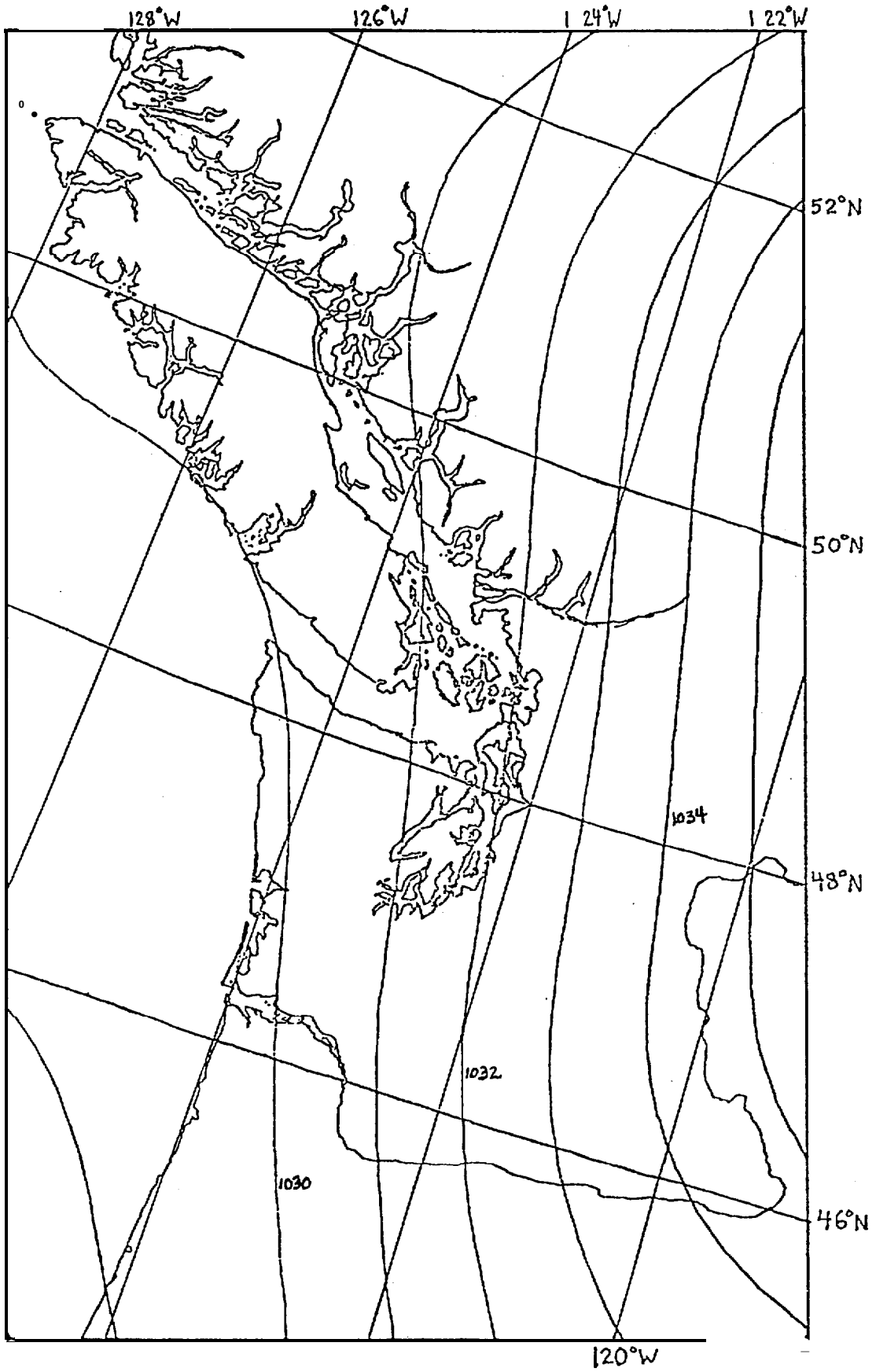


Figure 16.

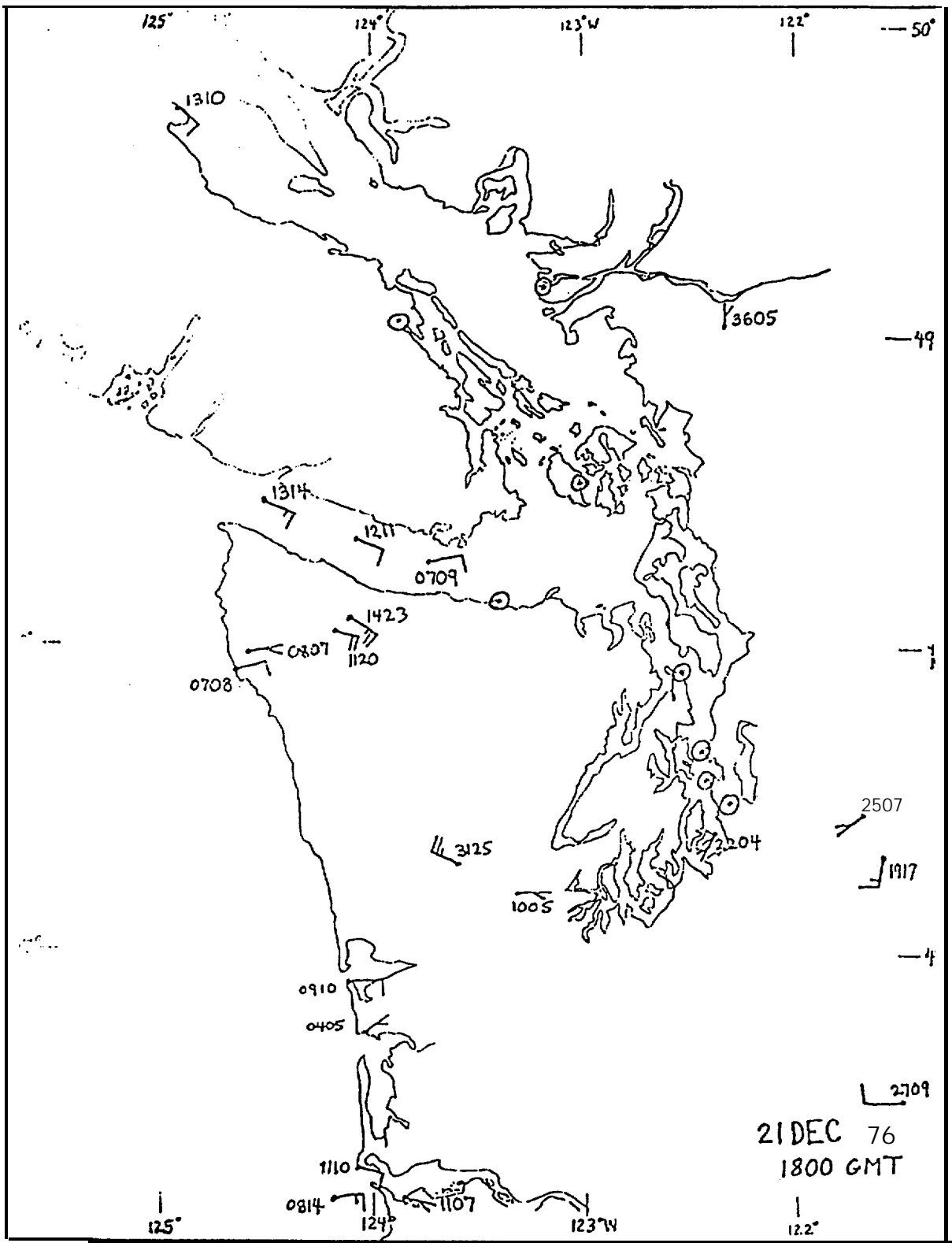
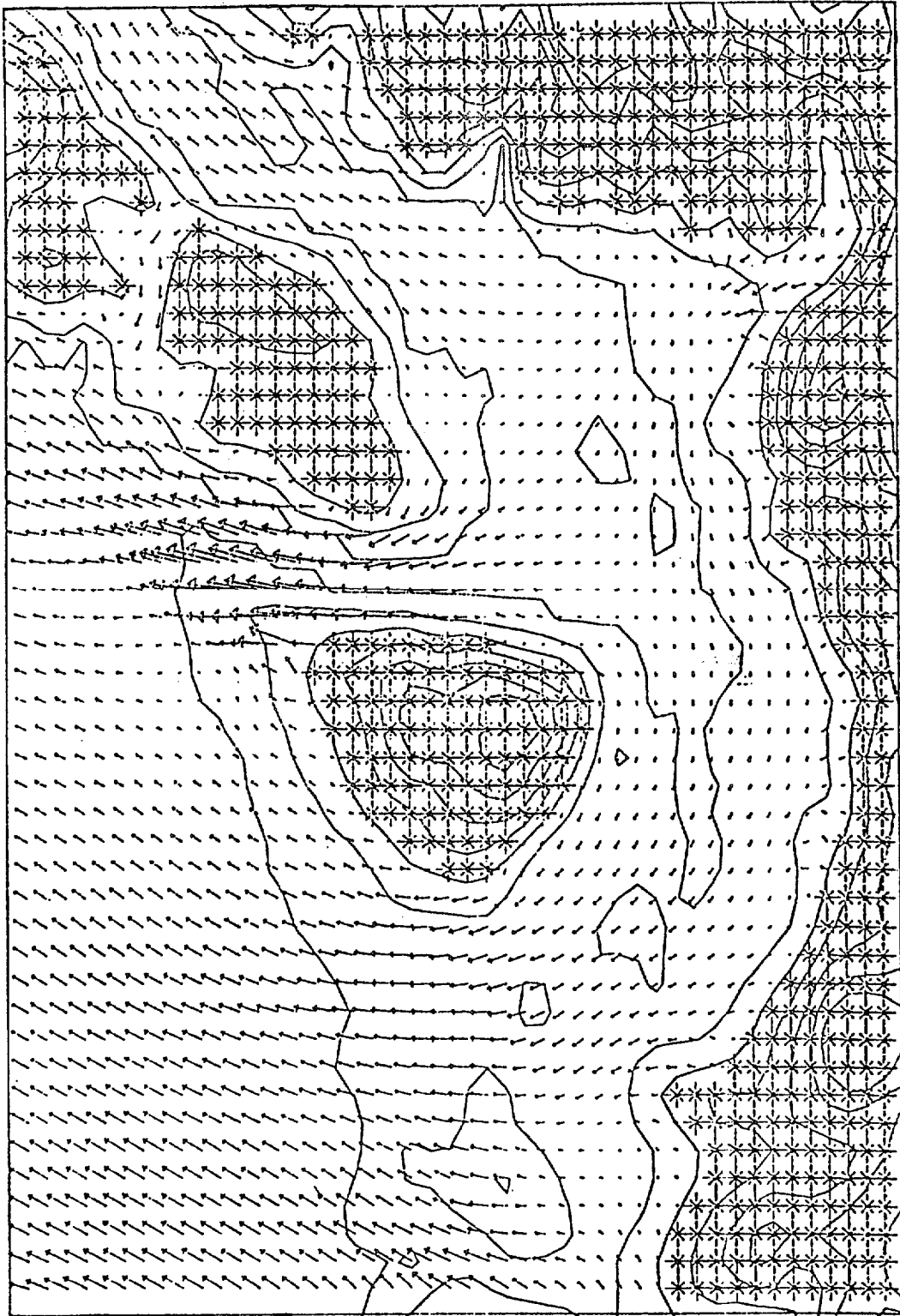


Figure 18.

VELOCITY VECTOR PLOT



4

10 METERS PER SECOND

Figure 19.

VELOCITY VECTOR PLOT

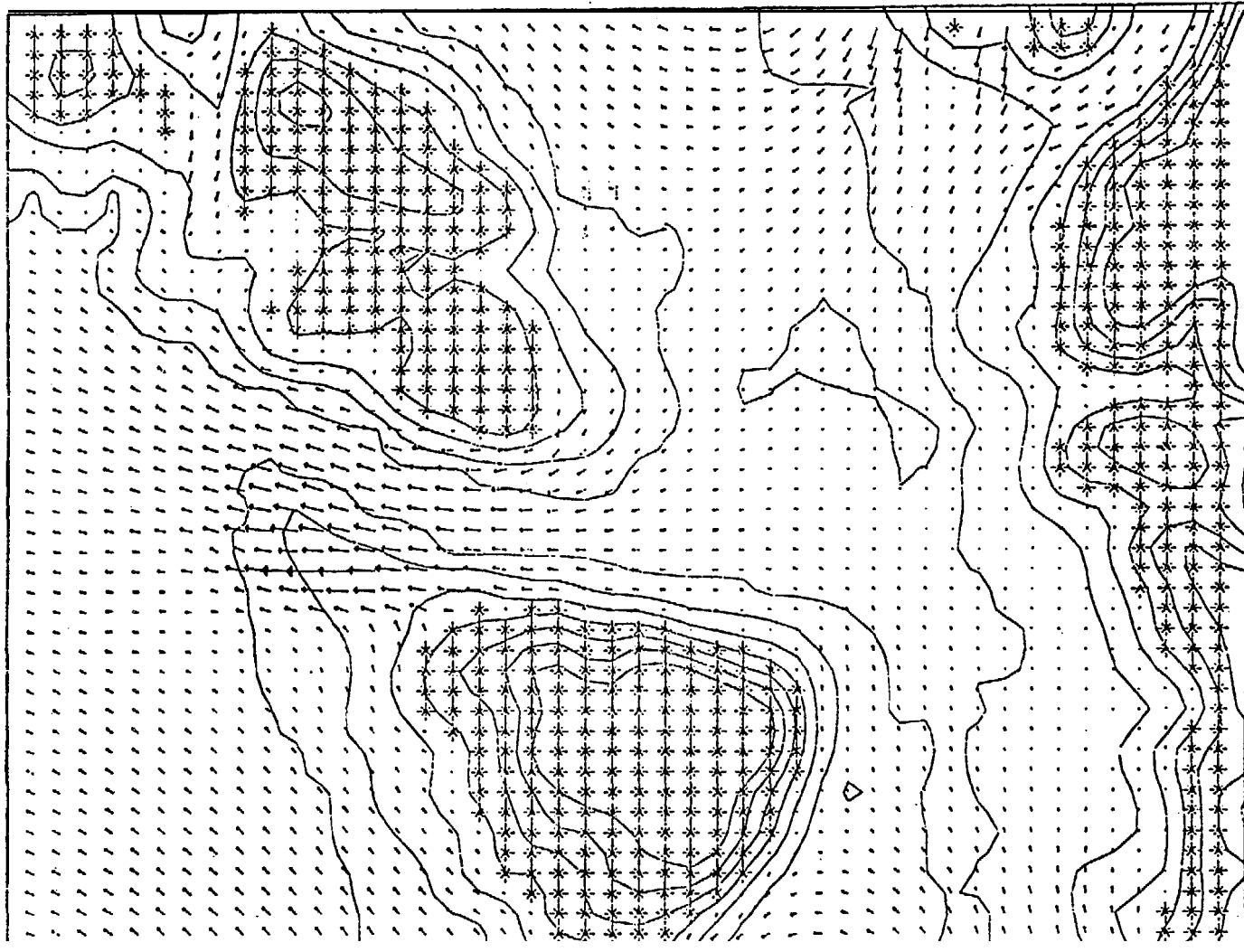


Figure 20.

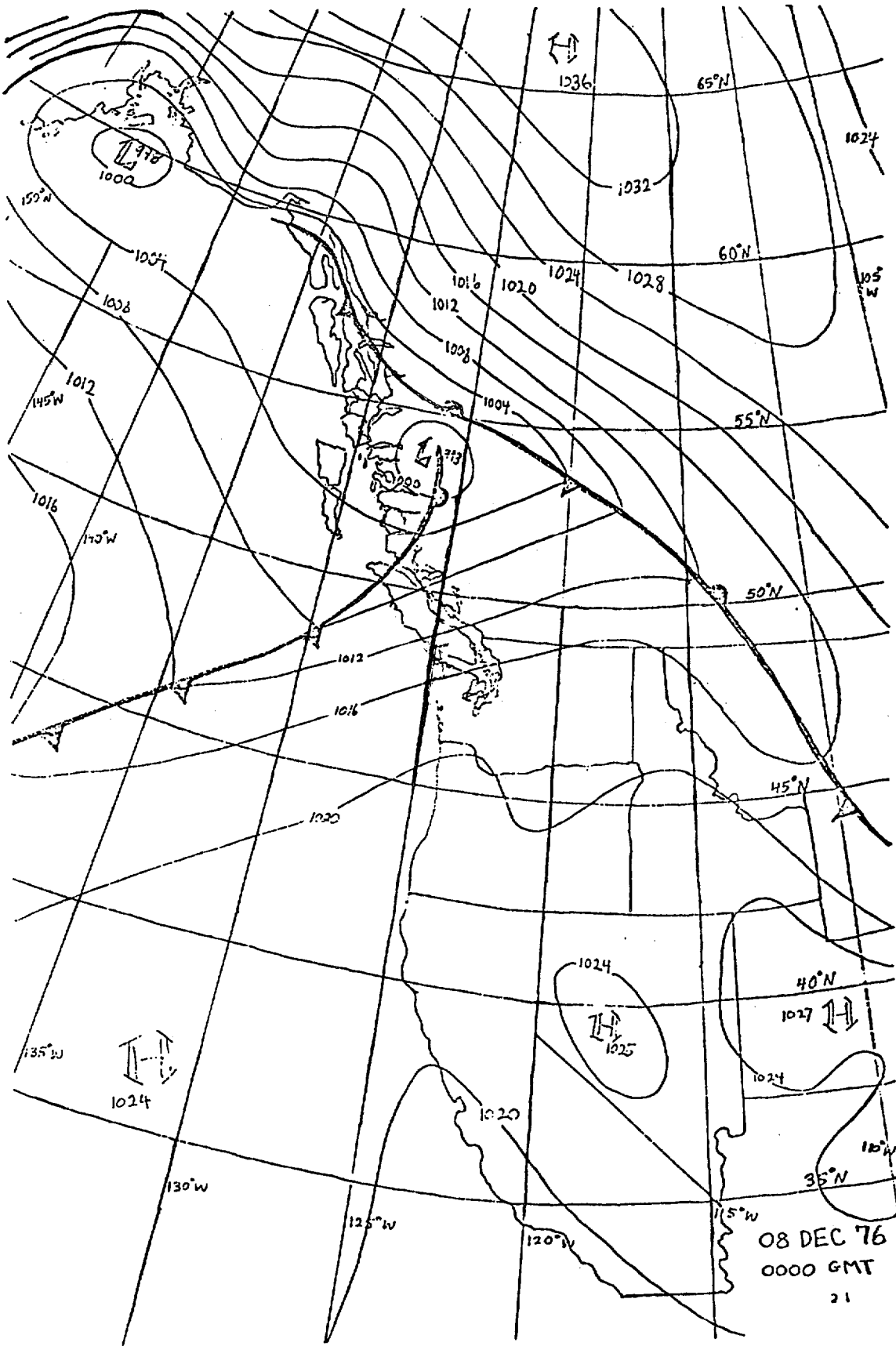


Figure 21.

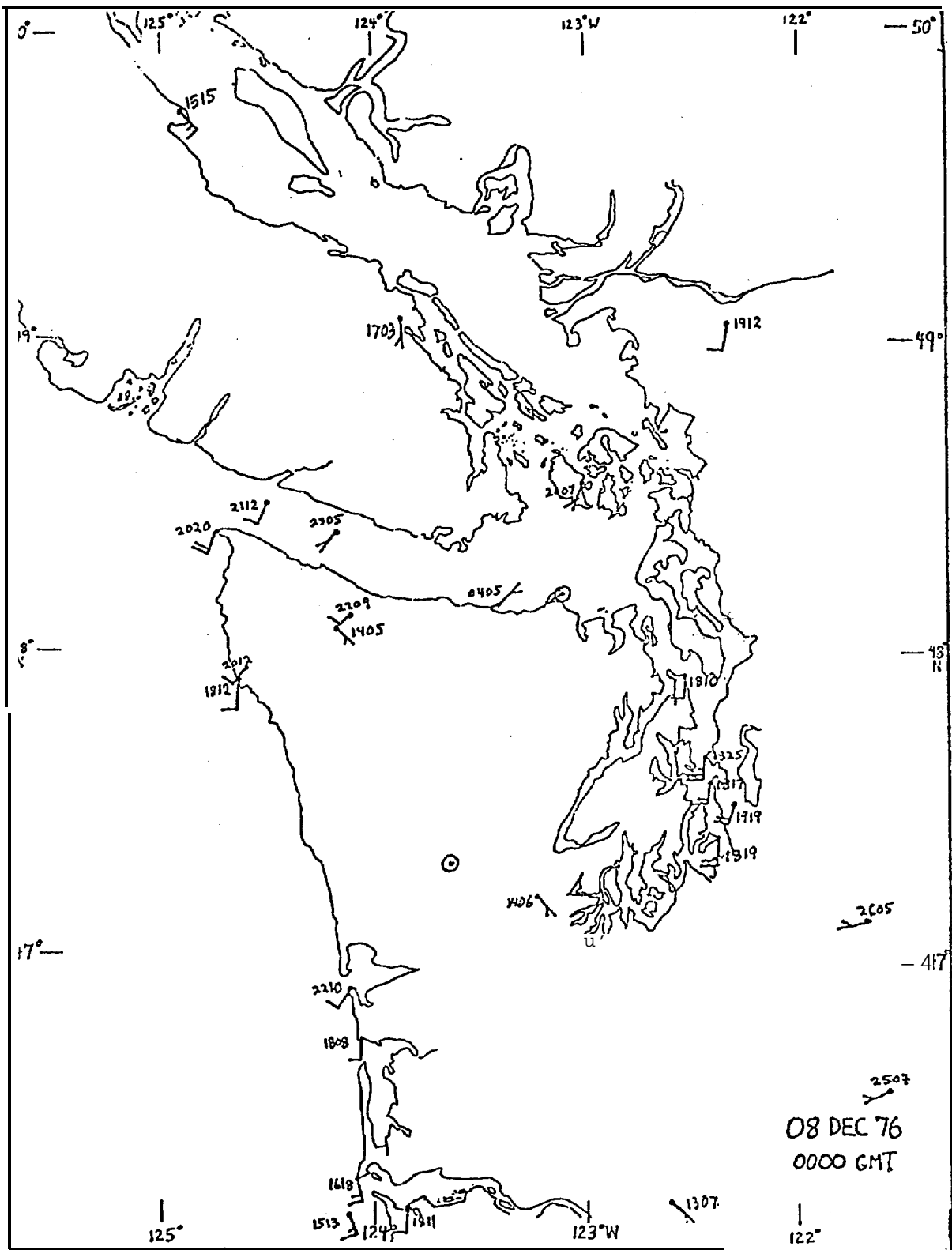


Figure 22.

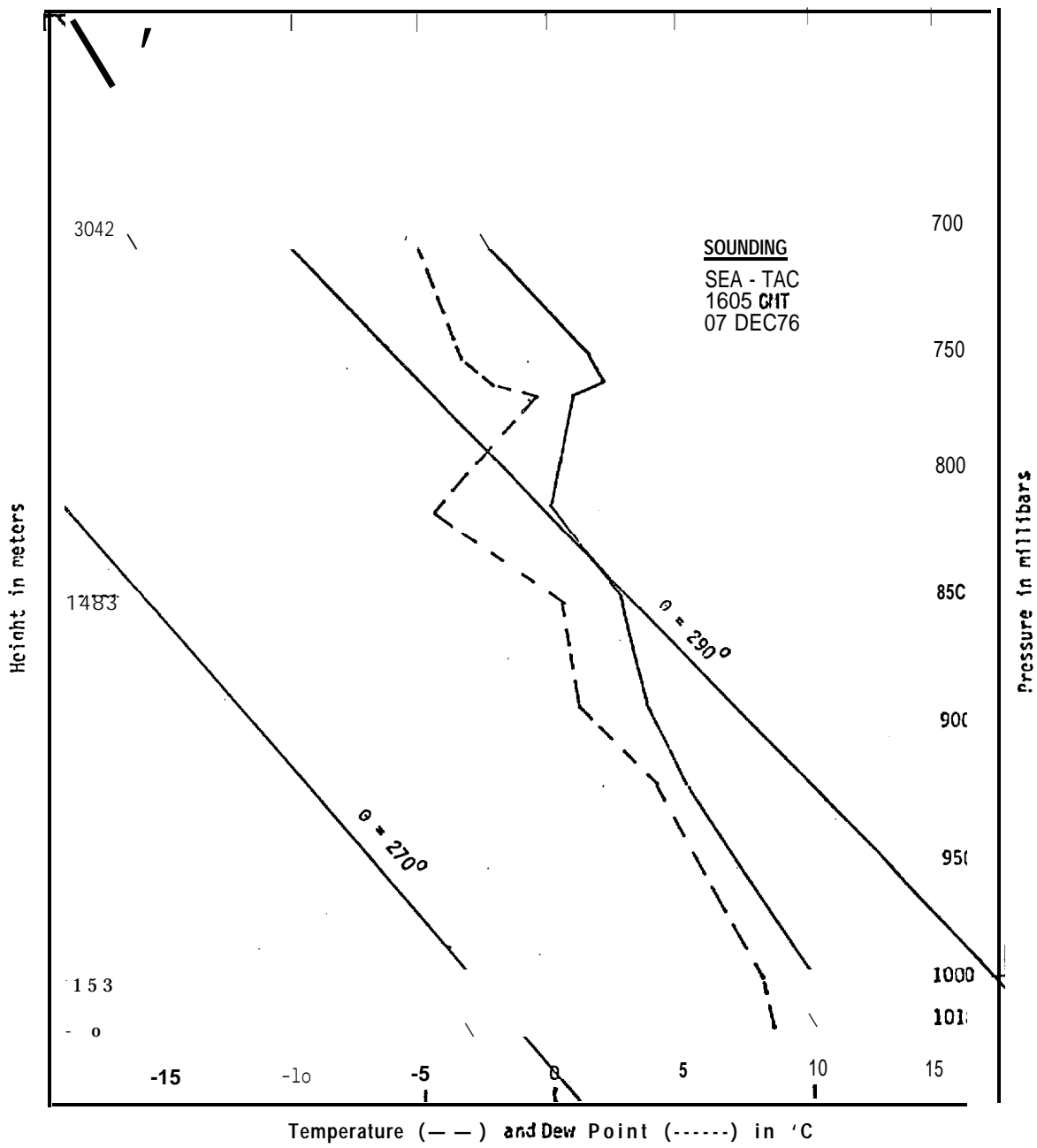


Figure 23.

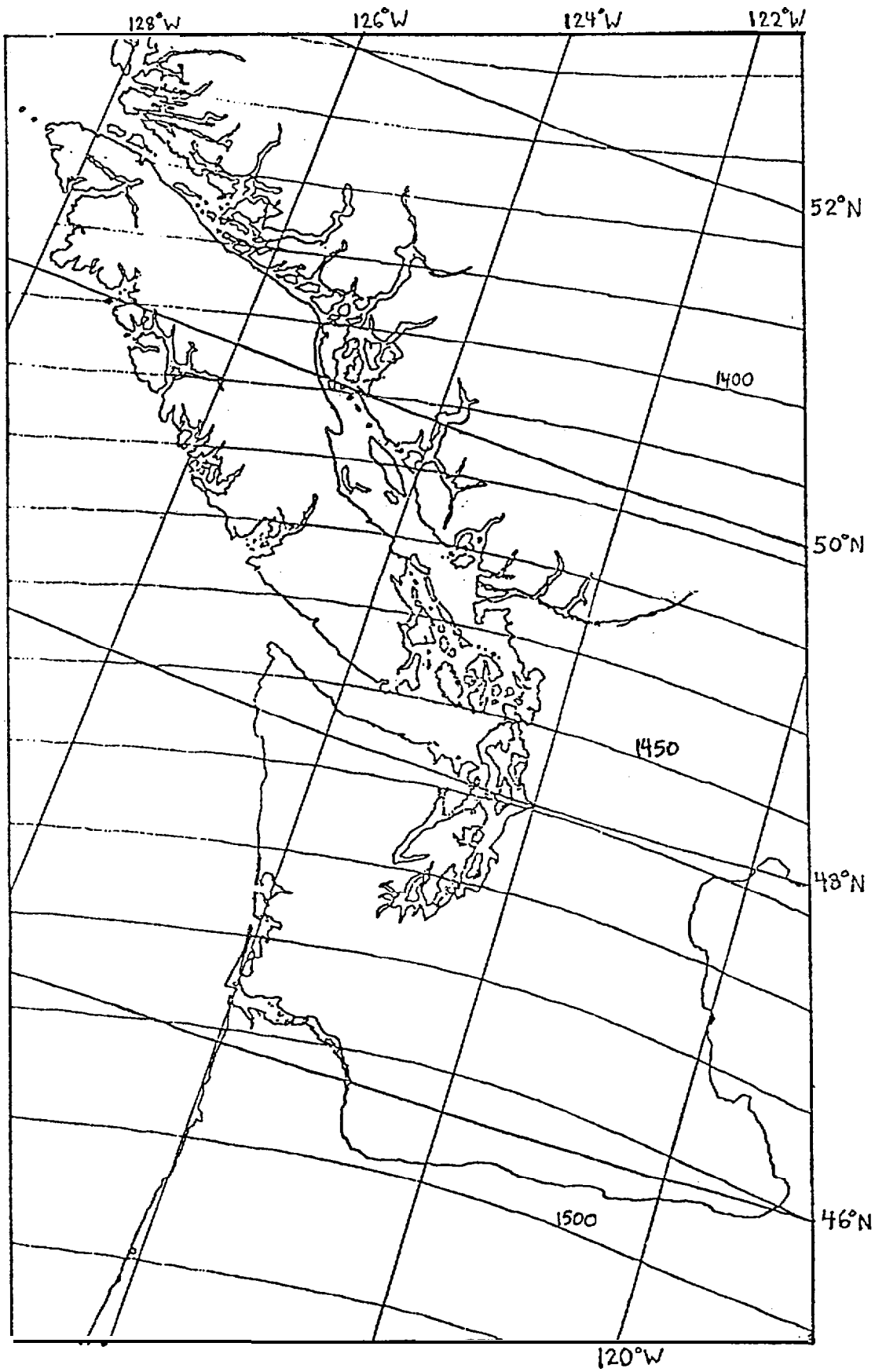


Figure 24.

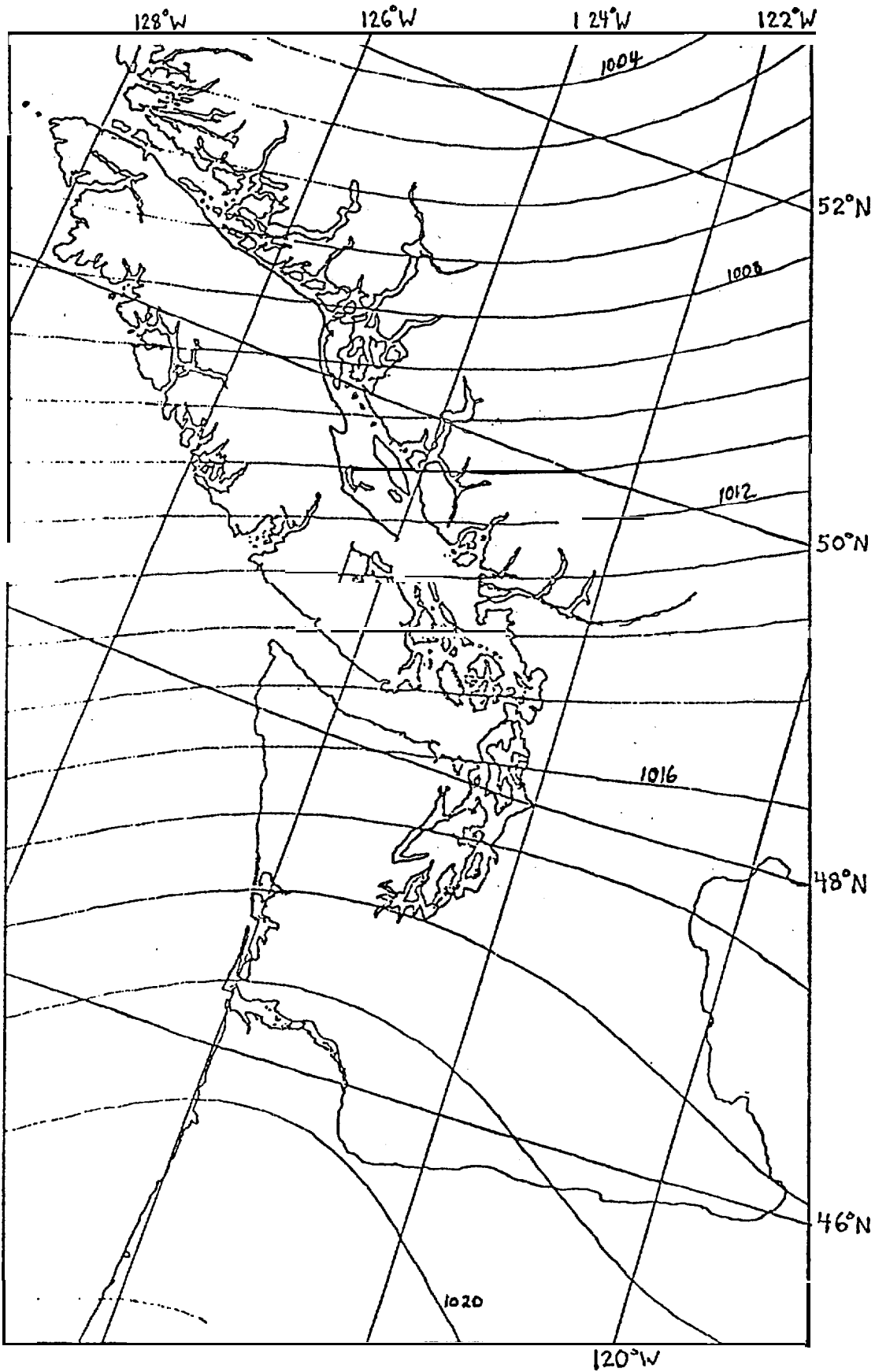


Figure 25.

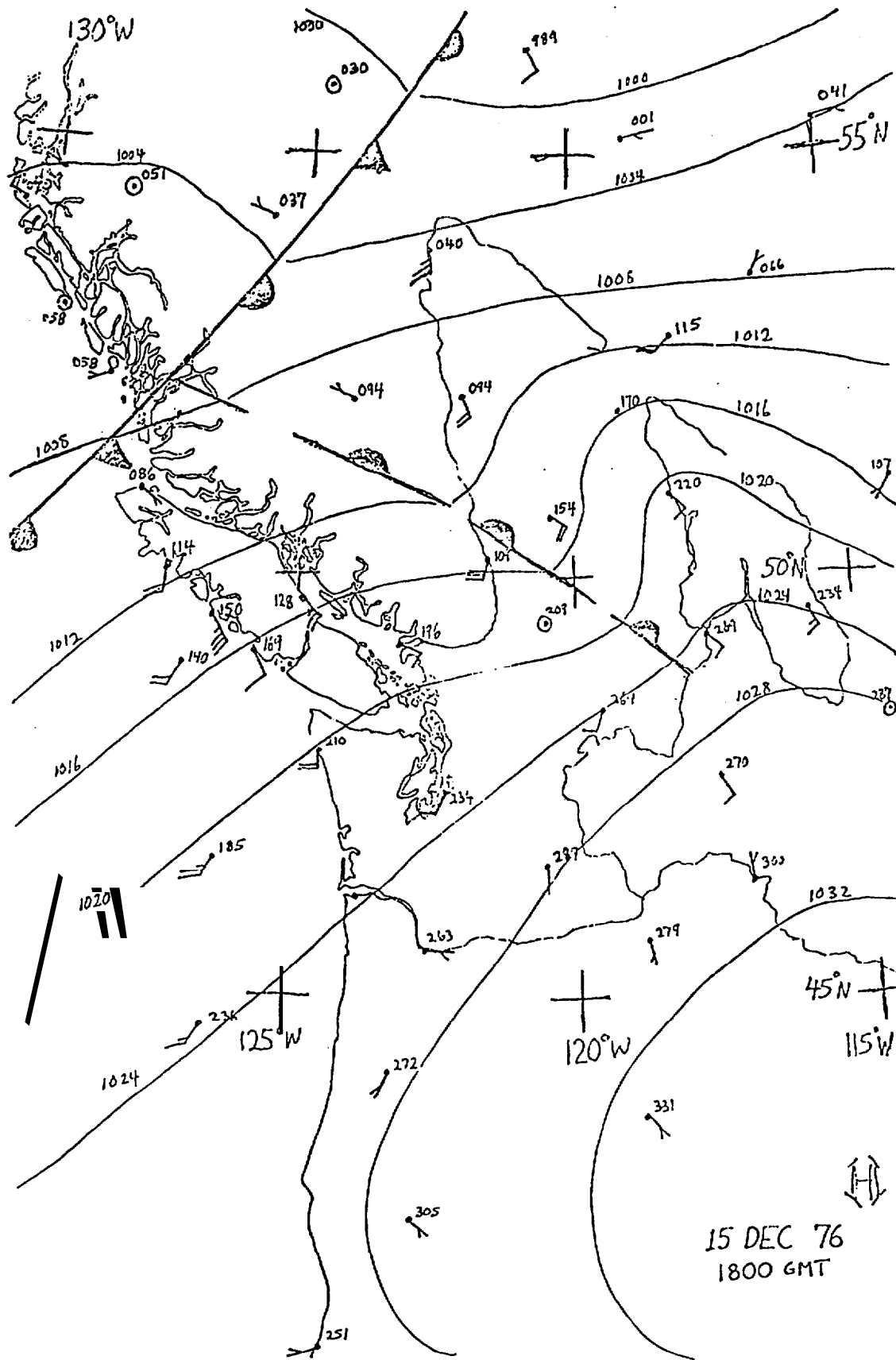


Figure 26.

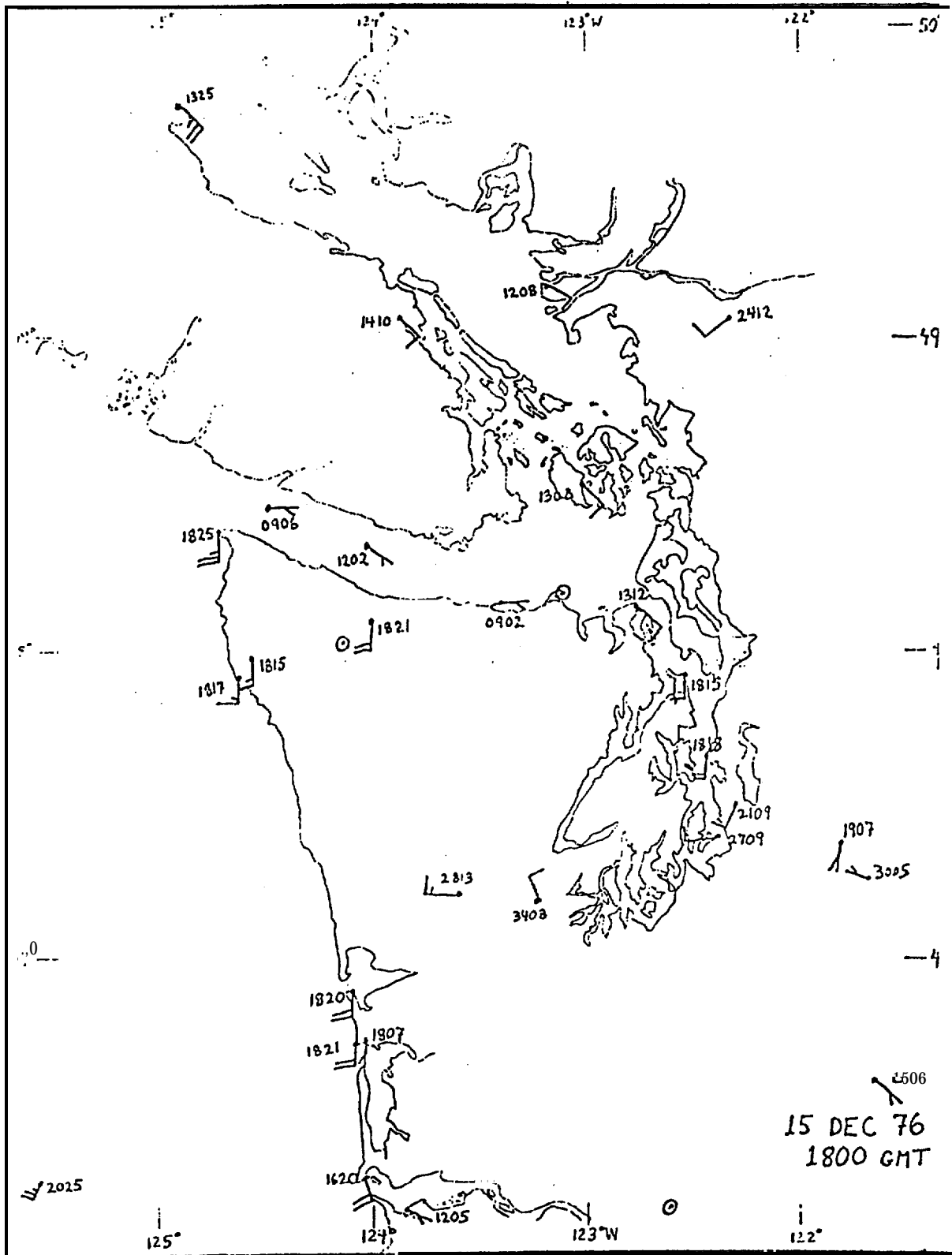
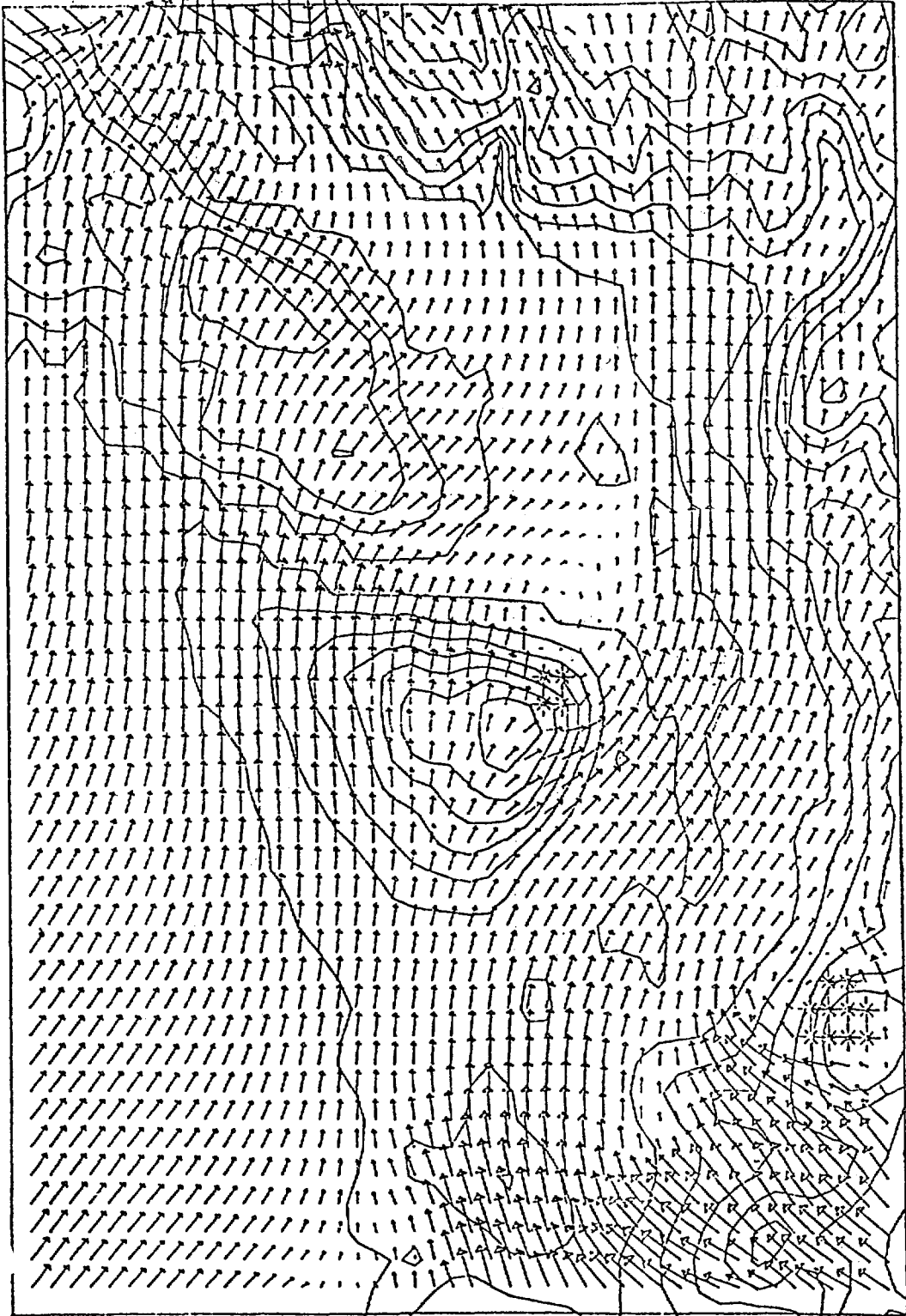


Figure 27.

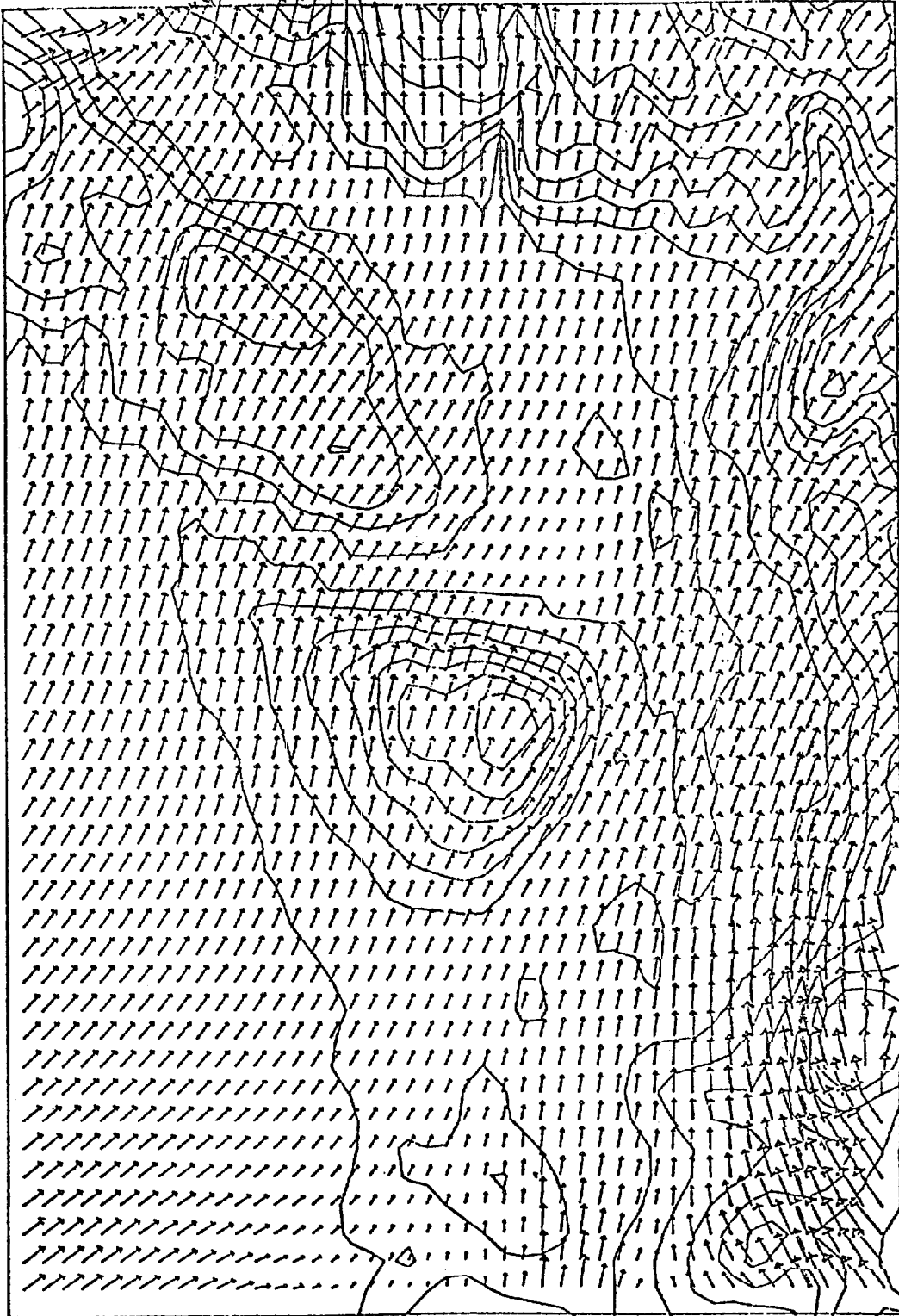
VELOCITY VECTOR PLOT



10 METERS PER SECOND

Figure 28.

VELOCITY VECTOR PLOT



10 METERS PER SECOND

Figure 29.

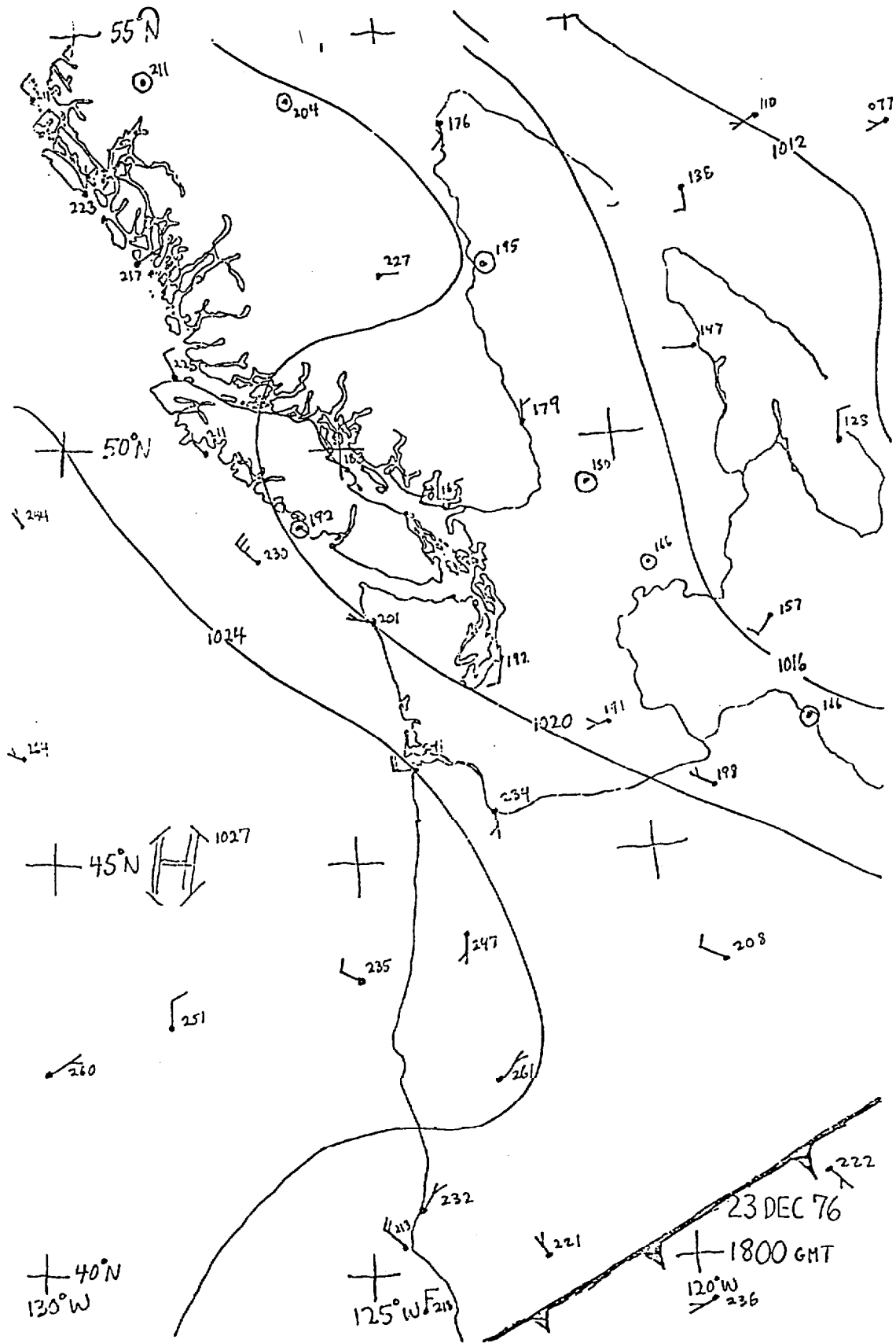


Figure 30.

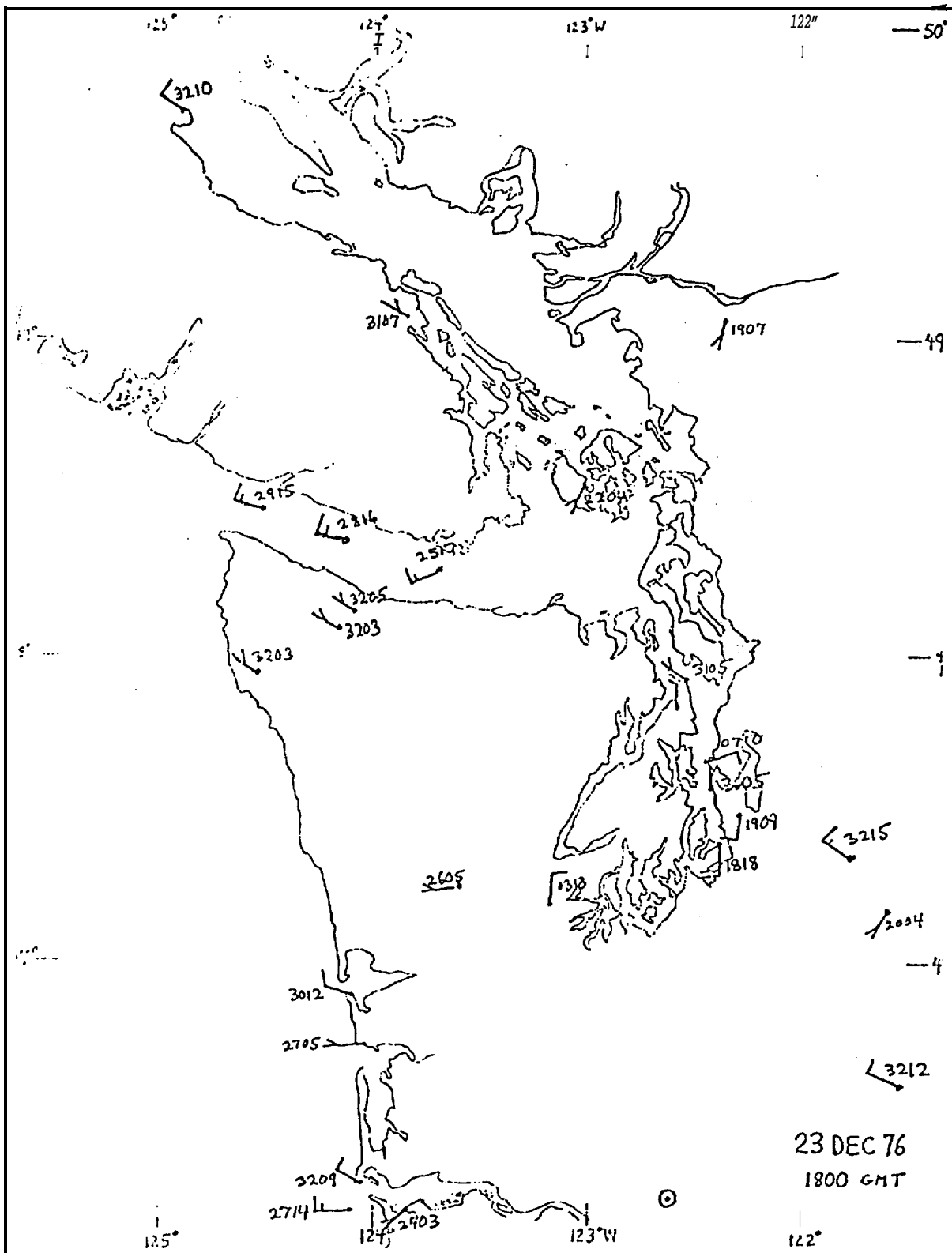


Figure 31.

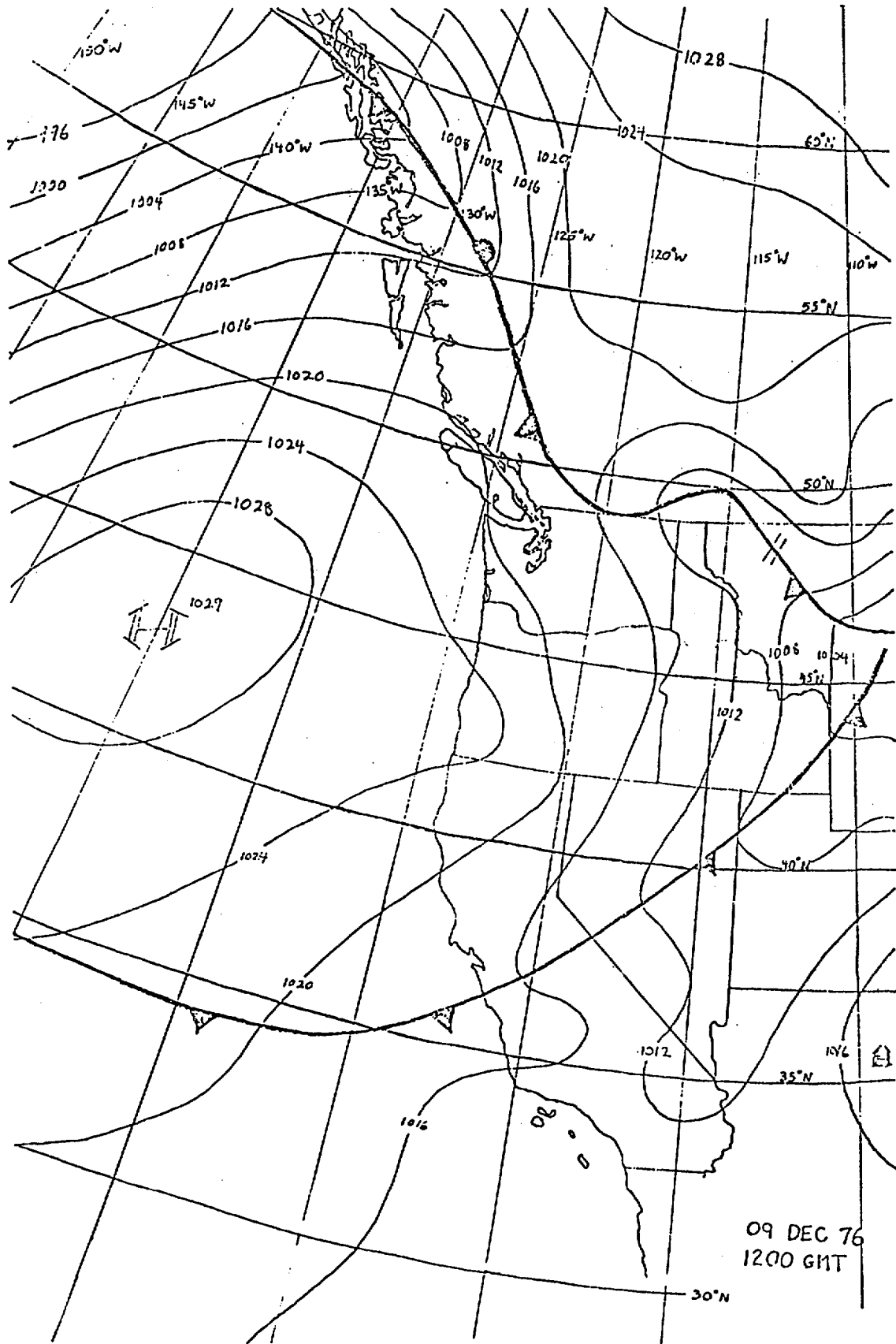


Figure 32.

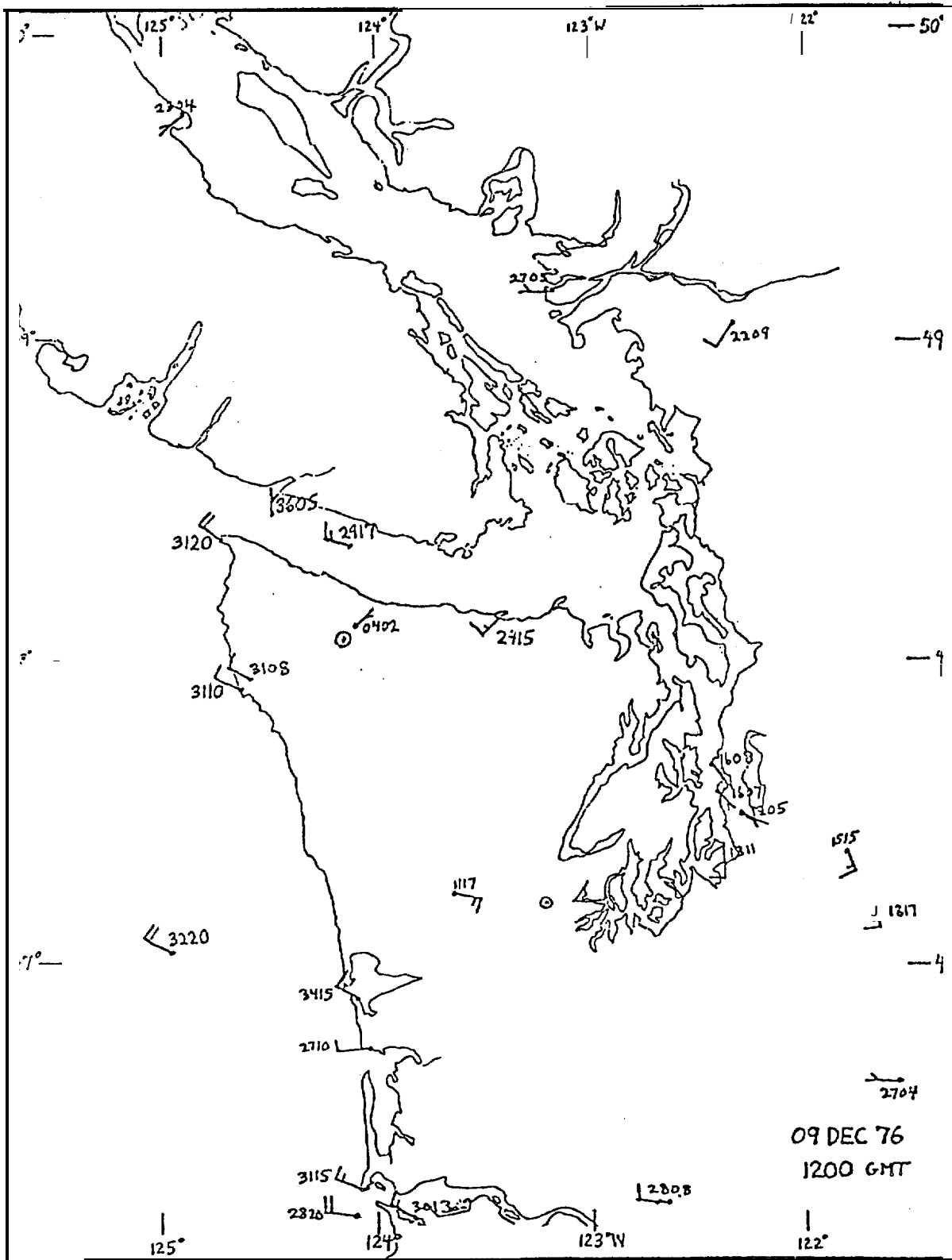


Figure 33.

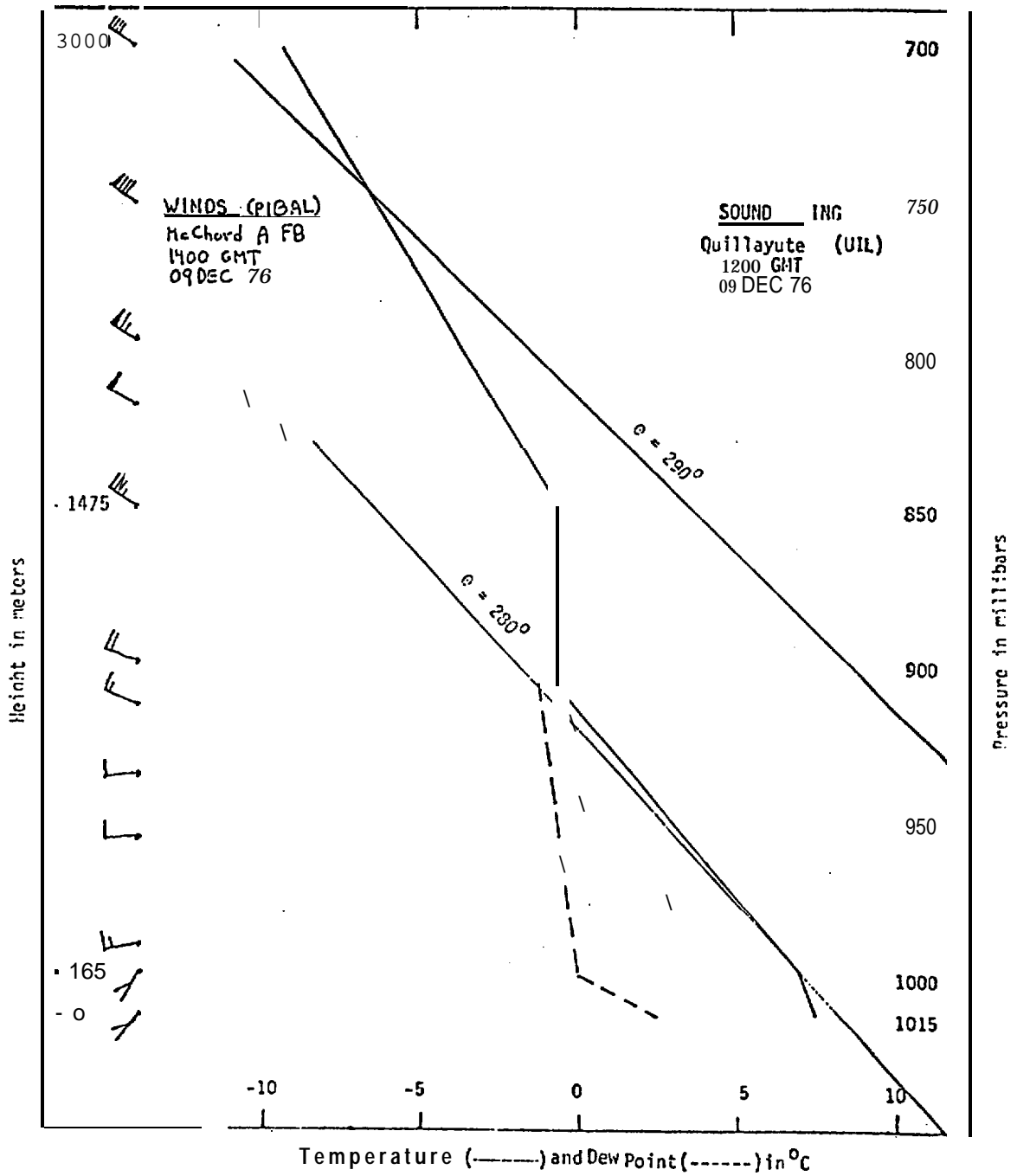


Figure 34.

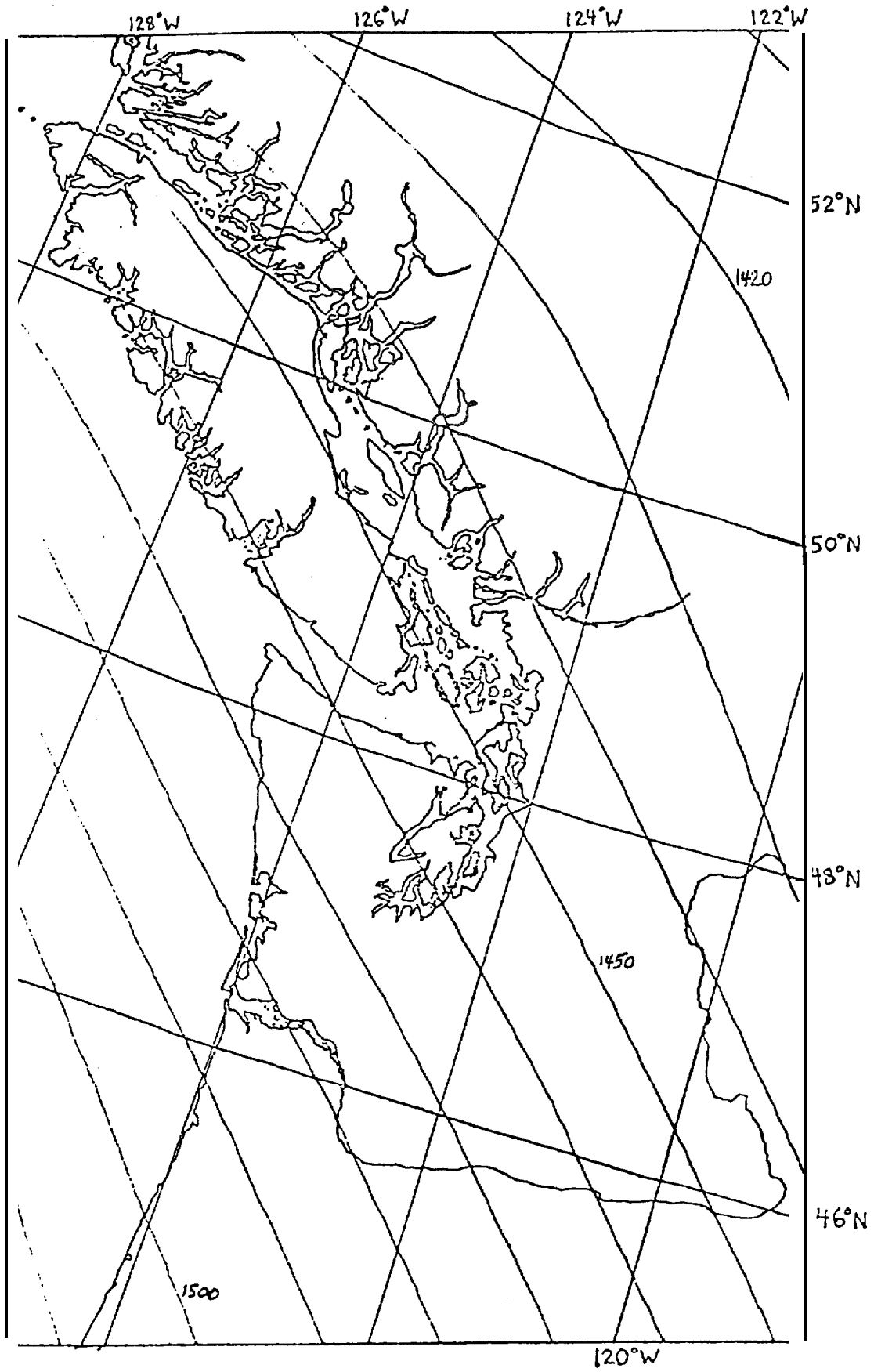


Figure 35.

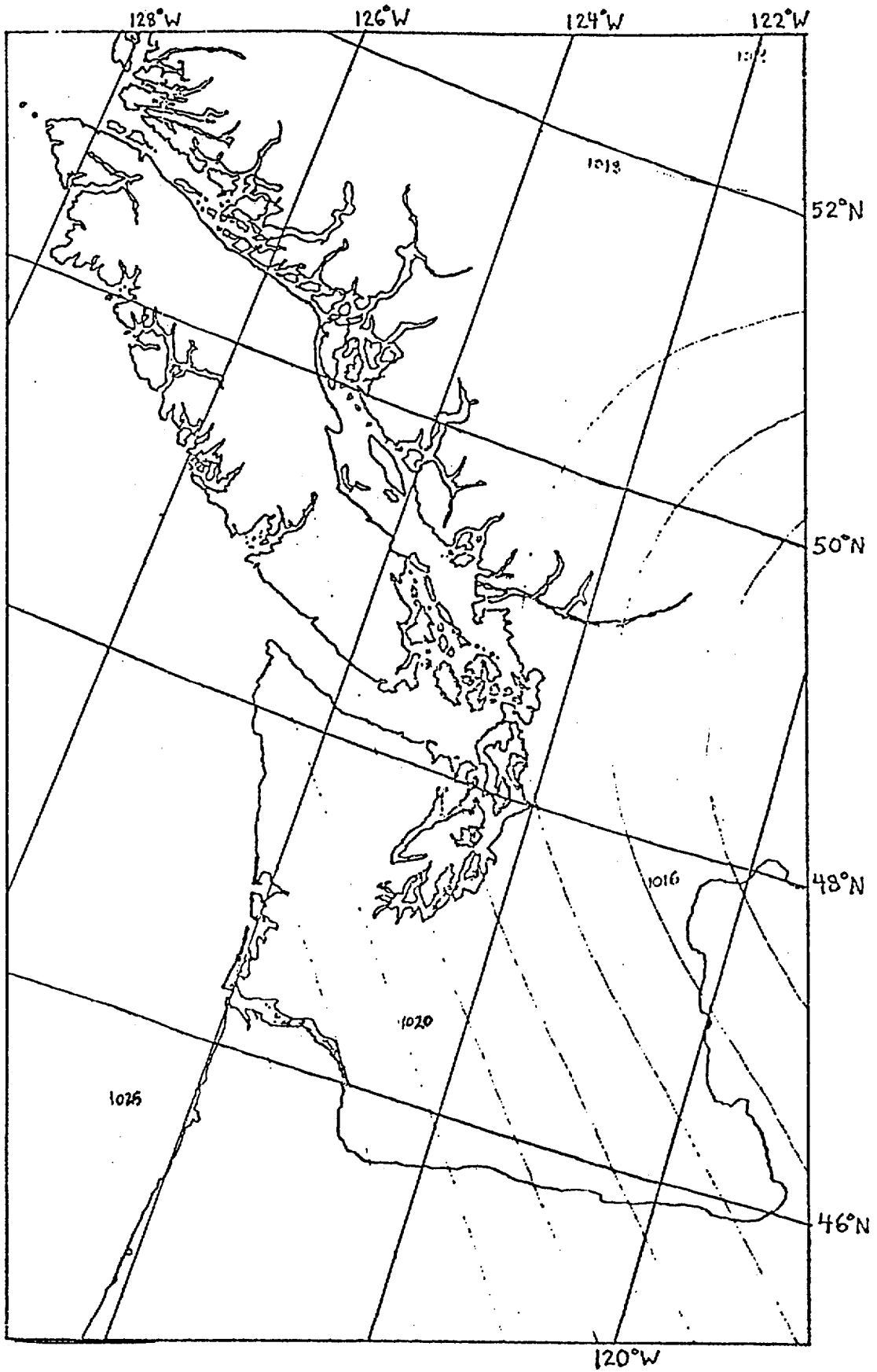
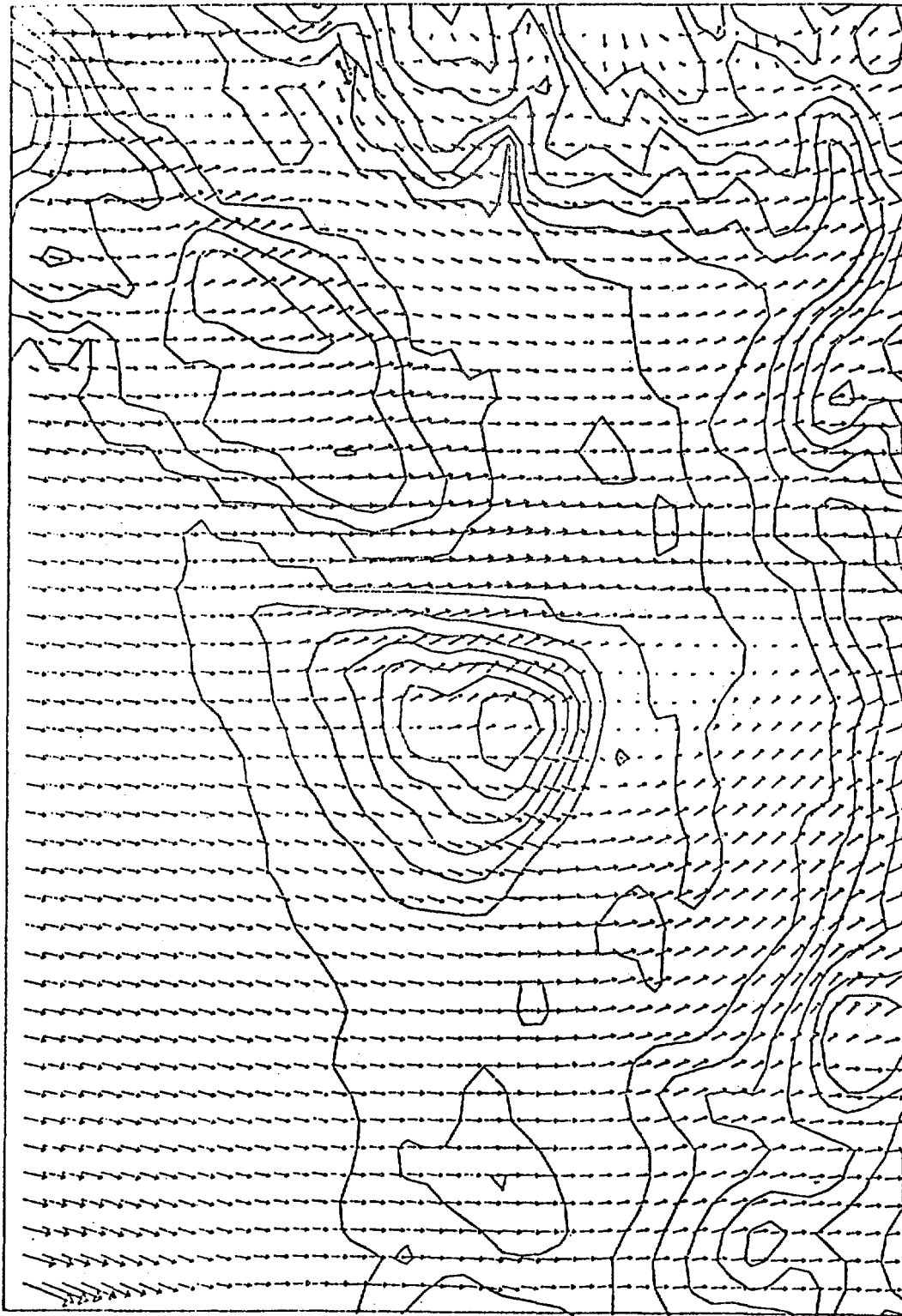


Figure 36.

VELOCITY VECTOR PLOT



→

10 METERS PER SECOND

Figure 37.